THESIS FOR THE DEGREE OF LICENTIATE OF ENGINEERING

Recycling of Steel Grinding Swarf via Production of Iron Chloride Coagulants for Water Treatment

THOMAS OTTINK

Department of Chemistry and Chemical Engineering

Chalmers University of Technology

Gothenburg, Sweden 2024

Recycling of Steel Grinding Swarf via Production of Iron Chloride Coagulants for Water Treatment

THOMAS OTTINK

Technical report no 2024:02

Department of Chemistry and Chemical Engineering
Chalmers University of Technology
SE-412 96 Gothenburg
Sweden
Telephone +46 (0)70-264-2796

Cover illustration: Concept for recycling of grinding swarf by Thomas Ottink

Printed by Chalmers digitaltryck
Gothenburg, Sweden 2024

Recycling of Steel Grinding Swarf via Production of Iron Chloride Coagulants for Water Treatment

Thomas Ottink
Industrial Materials Recycling
Department of Chemistry and Chemical Engineering
Chalmers University of Technology

Abstract

Grinding swarf is a hazardous waste generated in the manufacturing industry when making products out of iron and steel. Annually 10-12 million tons are generated worldwide, and these numbers are projected to grow with steel production and industrialization of developing countries. Waste management of grinding swarf is challenging because of its low value, heterogeneity, flammability and small quantities produced in many workshops and as such, landfilling is today widespread. The swarf is usually contaminated by lubricant oils which classifies it as hazardous waste and requires specialized landfills for disposal. This not only makes current waste management expensive and unsustainable, but also forms an environmental threat from leached metals and lubricants ending up in soil and groundwater.

Since steel grinding swarf predominantly consists of iron, the aim of this thesis was to investigate whether it could be used as raw material in production of iron based coagulants for water treatment. Hydrometallurgy was used to extract iron from swarf by leaching with hydrochloric acid and separating the formed iron chloride solution from metal impurities by precipitation and filtration. Each step of the process was designed and optimized to find simple yet flexible solutions to make the recycling process economically feasible, and capable of handling variations in the grinding swarf.

A two-step method was proposed based on completely dissolving iron in the swarf at 60°C and pH ≤2 for 3 h, and thereafter reducing the acid concentration to pH 4 for 1 h to precipitate any leached impurities. This guarantees complete separation of Al, Cr and Mo from the solution by hydrolysis, and can to a large extent also remove Co, Cu and Ni by cementation. Lubricating oils are flocculated by solids in the slurry and can therefore also be removed by filtration.

A 3.8 M $FeCl_2$ solution was produced which conformed to the highest purity standards for drinking water coagulants and was considered to be a good precursor for $FeCl_3$ production. Around 30 kg hydrogen gas are also generated per ton of swarf recycled which can provide additional value in recycling if captured. Besides these products, the process also generated solid leaching residues which were determined to have potential application in high alloy steel production.

Keywords: Hazardous waste, Hydrometallurgy, Leaching, Ferric Chloride, Water Treatment

List of Publications and Manuscripts

This thesis is based on the following paper, manuscript and patent application.

Paper I

Ottink, T., Vieceli, N., Foreman, M. R. S., & Petranikova, M. (2022). Novel approach to recycling of steel swarf using hydrometallurgy. *Resources, Conservation and Recycling*, *185*, 106450.

Contribution: Main author and all experimental work.

Manuscript

Ottink, T., Petranikova, M. Recycling of steel grinding swarf via production of high purity iron chloride solutions and hydrogen gas

Submitted to Journal of Hazardous Materials

Contribution: Main author and all experimental work.

Patent

Ottink, T., Petranikova, M. Process for recycling steel swarf to produce an iron chloride solution, application number 2351066-2

Contribution: Technical description details, experimental work and figures.

Table of Contents

Abbreviations and definitions

a	Chemical activity
ANOVA	Analysis of variance
cBN	Cubic boron nitride
D	Diameter
DOE	Design of experiments
EU	European Union
F	Faraday constant
FCC	Face centred cubic factorial design
ICP-OES	Inductively Coupled Plasma Optical Emission Spectroscopy
IEA	International Energy Agency
K	Chemical equilibrium constant
LOD	Limit of detection
LOF	Lack of fit
L/S	Initial liquid to solid ratio
Q	Chemical reaction quotient
R	Gas constant
Ri	Recirculation step
rpm	Rotations per minute
RSD	Relative standard deviation
scCO2	Supercritical carbon dioxide
SDS	Safety data sheet
SiC	Silicon carbide
STP	Standard temperature and pressure
T	Temperature
TC	Total carbon
wt-%	Weight percentage
XRD	X-ray diffraction
%E	Percentage extracted
ΔG	Gibbs free energy
ΔH	Molar enthalpy
ΔS	Molar entropy
β	Cumulative equilibrium constant
γ	Activity coefficient

1 Introduction

Iron and steel are one of the most important materials in the industrialization of our society and can today be found everywhere around us. Due to its diversity, iron has applications in everything from cast iron in automobiles and construction, to stainless steel in home appliances. Iron and steel production is regarded as a symbol of technological development and the global production is expected to increase with the growth of developing countries [1, 2]. Due to recent accelerated economic advances of highly populated countries such as China and India, global crude steel production has doubled to an annual production of nearly 2 billion tons in the past 20 years and is projected to increase to 2.5 billion tons within the century [3, 4].

With this constant growth, questions about the steel industry's sustainability have become increasingly important in the past decades. Iron production requires a reduction from its oxide forms found in ores. This is today achieved by carbothermic reduction using coke and large amounts of energy which are mainly supplied by fossil fuels [2]. As a consequence, steel industry is today responsible for 10% of global energy related CO_2 emissions according to the International Energy Agency (IEA) [1]. To reduce this footprint, production from scrap is expected to increase due to its lower energy demand [5]. However, as limited scrap is available on the market and competition for scrap is expected to increase, primary production from ore will still be prevalent in the foreseeable future. Large efforts are made in replacing fossil fuels with hydrogen gas for iron reduction and as an energy source [2, 6]. These technologies still at an early stage but are expected to dominate the market between 2030 and 2050 [4].

The steel value chain starts at the blast furnace where ore is reduced to pig iron. Iron and scrap then are processed into steel in various furnaces and depending on what alloying elements are added, different product grades can be obtained of which low alloy commodity steels and cast iron are the most common [7]. Specialty steels such as stainless and high-speed steels have higher alloying element contents and are produced in lower quantities. Steel from the mill then needs to be shaped into a marketable product which is done at foundries and manufacturers. At the foundry, steel is cast into a mould and further shaped using machining processes such as turning and milling. Further machining and surface finishing by grinding and polishing is usually done at the manufacturing site before assembly of the final product.

In each of the steps of the value chain, considerable amounts of byproducts and waste are generated which need to be managed to prevent environmental pollution. The steel industry alone generates around 450-500 kg of byproducts per ton of steel with main fractions including slag, furnace dusts and sludges [8]. Foundries also produce furnace dusts and large quantities of waste sand from the casting process [9]. The machining processes which are used extensively in foundries and manufacturing and to some degree the steel industry, produce large volumes of waste lubricants and a type of metallic scrap called swarf [10, 11]. Swarf comes in various shapes and sizes and its recyclability depends on the machining process it was generated in.

A machining process usually contains three main elements: a workpiece that needs to be shaped, a tool for removing material from the workpiece, and a cutting fluid for cooling, lubrication and washing away metal chips. Materials from the workpiece and tool end up together with cutting fluids and hydraulic oils from surrounding machinery to form a sludge which is classified as a hazardous waste due to mineral oils and harmful additives in the cutting fluids [12, 13]. Larger swarf pieces generated by cutting, milling, turning, etc. are easy to separate from the sludge and can often be reclassified as non-hazardous waste and recycled as scrap within the steel value chain. Grinding swarf on the other hand has a greater capacity to retain cutting fluids and is prone to oxidation which can cause it to self-ignite [14]. Consequently, grinding swarf is today generally classified as hazardous waste (EU list of waste 12 01 18) [13, 15].

Grinding swarf is generated both at larger manufacturer sites and by smaller workshops and quantifying waste volumes is nearly impossible. An estimate based on the yearly global cutting fluid consumption suggested volumes of 2.3-5.8 million tons of grinding swarf in 2006 [16]. These numbers are in line with volumes reported by the German industry of 250 thousand tons in 1997 when related to crude steel production and indicate that the grindings swarf production is around 5-6 kg/ton steel [3, 15]. With the recent doubling in steel production, current volumes can therefore be expected to be around 10-12 million tons per year.

With a growing awareness for sustainability and circularity within manufacturing, the demand for a waste management strategy for grinding swarf is raised. Manufacturers have no use for swarf internally and are dependent on third parties for waste management. Recycling options are limited and require good cooperation across multiple actors which is hard to realize. Moreover, existing collaborations can, and have been known to stop abruptly due to fires caused by swarf in storage [14]. This often leaves no other alternative than incineration and/or landfilling which comes with progressively higher fees for hazardous waste [17].

Thus, a new reliable, flexible and economically competitive approach for recycling has to be developed. Since most swarf on the market consists of low alloy steel, its inherent value is low, making development of a new recycling process challenging. One way to overcome this problem is to make valuable products for other industries.

1.1 Aim and scope

The aim of this thesis is to investigate a hydrometallurgical approach for recycling of swarf by producing iron chloride solutions with intended use as a coagulant in water purification. The focus will be on minimizing chemical use and processing to make the recycling economically competitive. Iron coagulants need to meet standards for trace metal impurities to be applicable in water treatment, and the European standards for iron chloride coagulants will be used as a guideline for assessment of the final product. For this reason, experimental work will also be limited to investigating low alloy steel grinding swarf.

2 Background

Grinding processes are widespread in manufacturing for removing defects and finishing surfaces from steel surfaces and as such, most machining businesses generate grinding sludge as a waste stream. The sludge consists of large volumes of cutting fluids mixed with particles from the workpiece and grinding wheel. Within manufacturing, there is an incentive to reuse the cutting fluids because of their value and disposal costs and as such, filtration, centrifugation and other solid-liquid separation techniques are today standard for internal fluid recycling. Grinding swarf is obtained as a byproduct in the fluid recovery.

Table 1: Typical compositions of grinding swarf [18].

Material	Content (wt-%)
Iron	50-80
Alloying elements	0-15
Abrasives	4-20
Oil	0.5-40
Water	0-30

The main components of grinding swarf are metal shavings, abrasives, binder from the grinding wheel, water and/or cutting oils [19]. Typical composition ranges for grinding swarf components from Irani et al. [18], are given in Table 1. Hydraulic leakage oils (tramp oil) from surrounding machinery may also end up in the grinding swarf leading to increased oil contents. The sponge-like structure of grinding swarf distinguishes it from other swarf types and makes it ideal for retaining these fluids. Typical cutting fluids and abrasives used in grinding processes are described in the following sections.

2.1 Cutting fluids

Cutting fluids are commonly used in various machining processes including grinding for cooling and lubrication [20]. The fluids protect the machining tool from wear by providing lubrication and cooling and help wash away chips while providing corrosion protection for the workpiece [10, 12]. Cutting fluids can be categorized into oil based and water-based fluids as shown in Figure 1, and usually contain various additives for improved performance.

Water based fluids are today most commonly used and are typically used in concentrations of 5-6% in water. These fluids can be divided into three sub-categories based on their oil content. Soluble oils contain >60% oil with surfactants to create a milky emulsion when mixed with water while synthetic fluids are free of oil and based on inorganic salts and amines and are transparent [12]. Semi-synthetic fluids are mixtures of soluble oil and synthetic fluids and as a result have a more complex composition. Common additives in water-based fluids are surfactants and defoamers to modify fluid properties and organic rust inhibitors to protect the steel surface from corroding. Straight oils are today mainly based on mineral oil and may contain additives to modify lubrication effects.

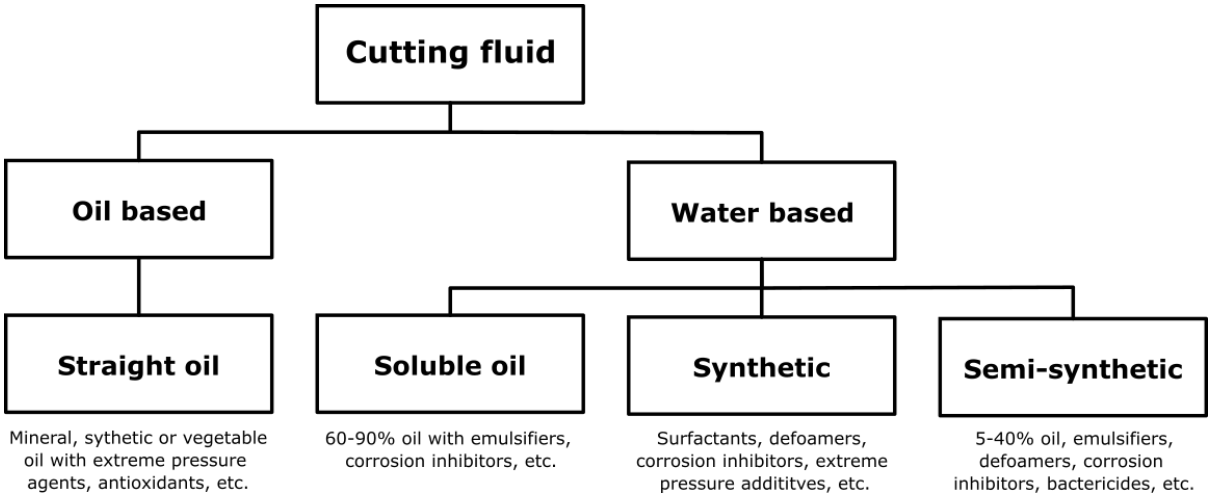

Figure 1: Categories of cutting fluids used in machining with common composition.

Large quantities of cutting fluids are used in the grinding process and many base oils and additives are a threat to aquatic life and human health [12]. Water based fluids are breeding ground for bacteria and are known to cause dermatitis and more serious health problems if metals from the workpiece are dissolved in the fluids [18].

2.2 Abrasives

Grinding wheels or discs that are used in the grinding process consist of abrasives materials that are held together or attached to a surface with ceramic or organic binder materials [21, 22]. The abrasive is selected based on price and application with hardness of the abrasives increasing with hardness of the steel. Some typical abrasives are shown in Figure 2.

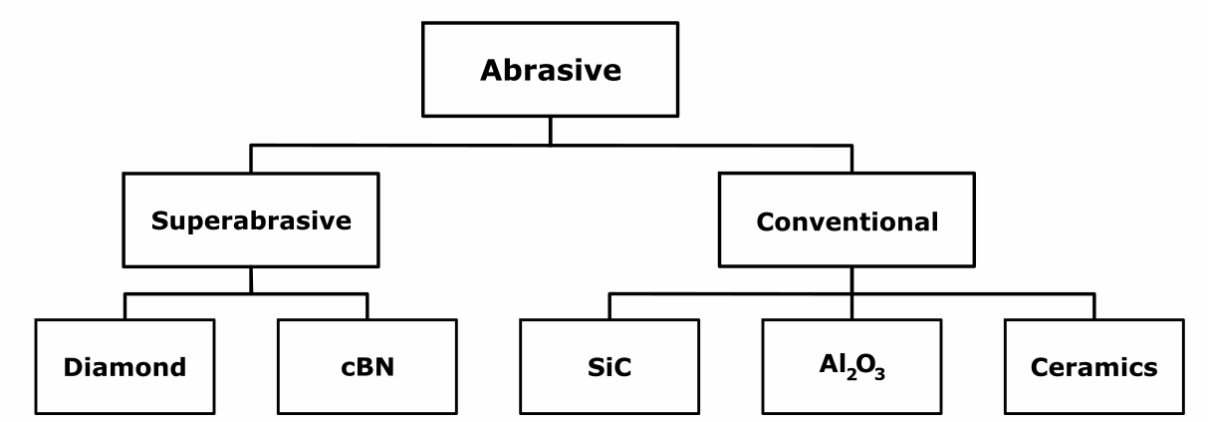

Figure 2: Some common abrasives used in industrial grinding processes with decreasing hardness from left to right.

Due to mechanical degradation, material is continuously released from grinding wheel and ends up together with the sludge. From a waste management perspective, the choice of abrasives is therefore crucial for the grinding swarf composition. Superabrasives generally degrade slowly and thus end up in the grinding swarf to a far lower extent while the softer, conventional grinding wheels need to be replaced regularly. This means that larger waste

volumes are generated when working with conventional wheels. Periodical dressing and resharpening of the wheels is required which can also lead to increased amounts of abrasives ending up in some swarf batches.

2.3 Swarf handling and waste management strategies

The near-endless combination of steels, cutting fluids and abrasives, and situation where grinding swarf production is spread out over many workshops makes waste handling exceptionally complex. This requires both good logistics and handling at individual sites to prevent discharge of swarf to the environment. The first steps in the handling are usually to lower the cutting fluid contents since high oil contents lead to classification of swarf as hazardous waste which entails large disposal fees of up to 1200 €/ton [13, 15]. Filtration is the primary technique for recovering swarf from grinding sludge and an example of industrial filtration equipment is shown in Figure 3.

Figure 3: Vacuum filtration (left) and briquetting of grinding swarf (right).

Filtered swarf usually has an oil content in the upper limits given in Table 1 and additional treatment is required to decrease the fluid content further. Common methods that can be used are centrifugation and briquetting [23]. Briquetting is also used for other swarf types and residual fluid contents of ≤5 can be achieved by mechanically pressing out fluids [24]. This also results in a more compact swarf that is more easily transported. While filtration is today more or less standard at larger manufacturers, briquetting is less common due to lack of economic incentive. Savings in cutting fluid are minimal and reclassification to non-hazardous waste is seldom guaranteed. Moreover, applications for dry grinding swarf are today limited to only a few options.

Recycling as scrap

The most logical alternative for grinding swarf is to recycle it as scrap. This is already practiced by internal recirculation within foundries where different types of swarf are remelted to produce new steel. Any oil residues are combusted in the furnaces while abrasives end up in the slag. However, not all furnaces are suitable for recycling since Al_2O_3 abrasives have been shown to damage the furnace lining in some cases [25]. Putting grinding swarf back into steel production also requires oil content below 3% to prevent burning and explosions [16], and high-quality briquetting to prevent swarf from crumbling back into a powder when charging and operating the furnace. Loose swarf may otherwise be carried with off-gases to form furnace dust which is a byproduct for steel mills and foundries.

Since variations in swarf compositions are common, consistent production of high-quality briquettes can be challenging. Previous investigations have shown that moisture contents above 2-3%, tramp oils and oxide layer formation prohibit good briquetting [23, 25]. One way to overcome this problem is to mix grinding swarf with larger swarf pieces or a binder material. This can also help with increasing swarf volumes, which is important since grinding swarf volumes alone are usually too low to be of interest for steel producers.

Filler in cement clinker

Another way to recycle grinding sludge and swarf is use as a filler in cement clinker production [26]. Small additions of up to 2% grinding sludge were shown to be feasible in replacement of virgin materials. The value of metals in the swarf is however lost in the process since the steel fraction is converted to oxides. High alloy swarf may also be less suitable for this application since valuable alloying elements are lost in the concrete and may form a potential hazard by leaching out over time.

Composting and incineration

A more unusual treatment of swarf is composting. To lower the organic content of the grinding swarf further after filtration, centrifugation or briquetting, composting can be applied to consume remaining oils and additives by microbes. Incineration serves a similar purpose but with energy recovery from combusted oil and metals. Both methods lead to reclassification of the swarf as non-hazardous waste. However, they also dramatically lower the value of the swarf since most metals are oxidized in the process, rendering it practically useless for anything but landfilling.

Landfilling

Landfilling is the last and least preferable option when none of the previously described alternatives are available. With a hazardous waste classification, grinding swarf has to be put in specialized landfills which comes with large disposal fees which increase with residual oil content. Landfilling is also a threat to the environment due to risks from leaching of cutting

fluids and metals into soil and groundwater [25]. Moreover, disposal also puts increased pressure on natural resources when materials are not recycled.

From a waste hierarchy perspective, recycling of grinding swarf as scrap is today the preferred option since the valuable steel fraction is reused. If this fails, use as a filler material or incineration should be applied to recover some materials or energy. Despite these alternatives, landfilling is today still widespread and new strategies are needed to increase recycling rates. From the manufacturers side, increased efforts should be made to reuse cutting fluids since this also increases the opportunities for metal recycling. Even if metals are disposed, economic returns from cutting fluid savings may in some cases justify investing in briquetting equipment, especially for larger producers. From a research standpoint, emphasis should be on developing new technologies for recycling the metal fraction in grinding swarf by making valuable products. This is needed to overcome the large investments that are required for developing and installing a recycling process.

2.4 Research and emerging technologies

In the past decades, research has mainly been focused on lowering the cutting fluid content of grinding swarf in order to recover oils and metals. Numerous efforts have been made on developing washing procedures with aqueous detergents solutions, solvents and supercritical CO_2 extraction (scCO2) [16, 27–30]. These studies have shown that oils adhere strongly to the steel surface and require some type of cleaning agent to be removed. As a consequence, multiple stages of washing and large volumes of solvent solutions are usually required which can lead to large wastewater or solvent discharge. However, reduction of cutting fluid contents below 3% can generally be achieved by washing making the swarf eligible for recycling in a steelmaking furnace.

Limited attention is often given to the reusability of the metal fraction and cutting fluids after washing. Briquetting is required for recycling in many steelmaking processes and washed swarf may be more difficult to briquette. This is especially true for aqueous washing processes where corrosion is likely when contacting swarf with water. Likewise, residual cutting fluids are usually complex mixtures of base oils, additives and organic degradation products and mixing these with a detergent is likely to ruin the possibility of reusing the lubricant for grinding. All parts of the lubricant should be recovered simultaneously to enable reuse, which is difficult due to of the varying properties of different additives.

More recent efforts by Hankel et al. and Großwendt et al. [15, 19], have focused on end use of dry swarf by using powder metallurgy techniques to create new steel. Magnetic separation and aqueous washing or scCO2 extraction were first used to separate abrasives and lubricants before sintering. More than 80% of the original Al_2O_3 and SiC abrasives were recovered and it was concluded that oil removal by scCO2 was preferable, since it doesn't produce any oily wastewater and avoids the need for drying compared with aqueous washing. Other studies have shown that up to 75% oil removal is possible with scCO2 [28]. The resulting steel was characterized and displayed a similar hardness but only 40% of the compressive strength of

the original steel workpiece due to non-metallurgically bonded Al_2O_3 and poor bonding of oxidized swarf surface in the steel matrix [15].

Since the main component of steel swarf is iron, an alternative strategy is to produce iron-based coagulants which can be used in water treatment [24]. This would promote recycling by creating a desirable and valuable product outside of the steel value chain.

2.5 Production and use of coagulants in water treatment

Flocculation and coagulation processes are used in wastewater treatment and drinking water purification to remove dissolved organic matter, suspended particles, phosphorous and heavy metals [31–33]. The methods are based on adding inorganic or organic chemicals early in water treatment to agglomerate (coagulate) and form larger aggregates (flocculate) with contaminants allowing them to be removed as a sludge by solid-liquid separation [34]. Combinations of chemical coagulants and flocculants are usually used since coagulants are most effective for precipitating suspended matter while flocculants can form polymers with precipitates to facilitate sludge separation.

While interest for using organic coagulants as a sustainable alternative is growing, inorganic salts such as ferric chloride ($FeCl_3$), ferric sulphate, aluminium sulphate, and poly aluminium chloride, are today most common [34, 35]. Iron based coagulants cover around 50% of the inorganic coagulant demand in Europe with around 2 million tons yearly [36]. The demand for sulphate or chloride-based coagulants varies greatly between countries and is largely based on raw material availability, regulations, preferences, and predispositions based historical incidents.

Ferric chloride is a versatile coagulant due to its ability to function both as an efficient coagulant and flocculant with main applications in water treatment and to some extent in catalysis, etching, etc. [37]. It is mainly sold as concentrated solutions of 40 wt-% $FeCl_3$ to minimize logistical costs and prevent freezing in colder climates. Ferrous chloride ($FeCl_2$) can also be used as coagulant but is less effective and has a smaller market. To allow use of iron chlorides as coagulants, trace metal impurity levels need to be low to prevent contamination of the treated water. Consequently, pure iron coagulants are today largely produced by dissolving high quality magnetite in concentrated hydrochloric acid. Steel industry byproducts such as spent pickle liquor can however also be used as raw materials depending on their purity [36, 37]. Any Fe(II) from primary or secondary production is usually oxidized to Fe(III) by chemical oxidation with chlorine, hydrogen peroxide, chlorate or pressurized oxygen.

3 Theory

3.1 Hydrometallurgy

Hydrometallurgy is a collection of methods involving processing of metals in aqueous media and is a technique that has been applied extensively in the mining industry but is also growing rapidly in the recycling and detoxification of waste materials [38]. Hydrometallurgy has several advantages over traditional pyrometallurgical processes in that it generally be performed at room temperature, can achieve higher purities and allows economic recovery of metals from low grade ores and low volume material streams. With our societies increasing energy demand and depletion of high-grade natural resources, hydrometallurgy is expected to play an important role in the future [39].

The first and most important step in any hydrometallurgical process is transfer of a desired metal from a solid phase to an aqueous medium by leaching using a lixiviant, usually an acid or base [38]. Mechanical or thermal pretreatment is commonly done prior to leaching to activate and make metals more susceptible to the leaching process [40]. Once the metals have been transferred to a leachate, they can be purified using various techniques such as solvent extraction, ion exchange and precipitation of impurities as hydroxides or by cementation. The desired final product is usually a solid and can be recovered from the aqueous solution by methods like crystallization, electrowinning, or spray pyrolysis.

3.2 Thermodynamics

Chemical reactions in general are driven by thermodynamics and basic modelling can help us predict and explain some of the phenomena observed in hydrometallurgical processes [38]. The main driving force behind changes in a thermodynamic system is the lowering of Gibbs free energy (ΔG) and is defined as

$$\Delta G = \Delta H - T\Delta S \tag{1}$$

Where T is the system temperature, ΔH is the molar enthalpy and ΔS the molar entropy change in the reaction. For any change in the state of the system to occur spontaneously, ΔG should be negative.

Thermodynamic systems strive to be in equilibrium where ΔG is minimized [38]. Thus, studying equilibria for chemical reactions is key in determining whether a reaction is likely to occur, and which species are likely to be formed at a given state. An analogue to Equation 1 for reactions is defined as

$$\Delta G_r = \Delta G_r^o + RT \ln Q \tag{2}$$

With ΔG° as the Gibbs free energy at standard temperature and pressure (STP) and R the gas constant. The reaction quotient Q is a measure of how far the system is from equilibrium and for an arbitrary reaction aA + bB ⇌ cC + dD, it is expressed as

$$Q = \frac{a_C^c a_D^d}{a_A^a a_B^b} \approx \frac{[C]^c[D]^d}{[A]^a[B]^b} \quad (3)$$

Where a_i is the chemical activity or effective concentration, and the right hand equality with concentrations generally holds for ideal solutions. Activities of pure solids or liquids are usually close to unity [38]. By definition, $\Delta G_r=0$ at equilibrium and Q is equal to the equilibrium constant K for the reaction. This simplifies Equation 2 to

$$\Delta G_r^o = -RT\, ln\, K \quad (4)$$

and gives us an expression for determining the equilibrium constant based on ΔG°. If for a given system Q<K, a net reaction will occur to form products while the reverse reaction is favoured when Q>K.

In an ideal solution, solute concentrations are sufficiently low to neglect molecular interactions between solutes, and activities can be approximated to concentrations of individual species [38]. However, in non-ideal electrolyte solutions which are more commonly encountered in hydrometallurgy, intermolecular solute interactions cannot be ignored. A measure of the electrolyte concentration is ionic strength.

$$I = \frac{1}{2}\sum_i^n C_i z_i^2 \quad (5)$$

Where C_i and z_i are the ion concentration and charge respectively. An aqueous solution is generally ideal when $I<10^{-5}$ M and at higher ionic strengths, activities can be estimated with Equation 6, with activity coefficients γ_i as a basis for deviation from ideality.

$$a_i = \gamma_i x_i \quad (6)$$

Here, x_i is the mole fraction of the solute and γ_i can be modelled using Debye-Hückel theory, specific ion theory (SIT), Pitzer's ion interaction, etc. [41, 42]. These models have shown to be accurate for calculating activity coefficients at moderate to high ionic strengths for monovalent salts. However, in very strong, mixed electrolyte solutions, these models are less reliable or no longer hold and empirical data is important in explaining deviations from ideality [43].

3.2.1 Electrochemical reactions

Many reactions in hydrometallurgy are inherently redox reactions since altering oxidation state can greatly influence the solubility and reactivity of a metal [38]. Electrochemical reactions involve transfer of electrons to or from species for reduction or oxidation respectively. An example is the half-cell reaction for the reduction of Fe from Fe(III) to Fe(II)

$$Fe^{3+} + e^- \rightleftharpoons Fe^{2+}$$

Electrons can be donated by another specie in the solution which is oxidized in a way that the overall electron transfer is balanced. The electron transfer is linked to electrochemical

potential *E* which is a measure of the work required for reduction or oxidation and is directly related to Gibbs free energy by

$$\Delta G_r^o = -nFE^o \tag{7}$$

Here, n is the number of transferred electrons and F is the Faraday constant. Standard reduction potentials E° are normally listed for 1 M electrolyte solutions unlike thermodynamic constants which are based on ideal dilute solutions. By inserting Equation 7 into Equation 2, a general expression for the electrochemical potential is obtained.

$$E = E° - \frac{RT}{nF} ln\, Q \tag{8}$$

This is the Nerst equation and is a direct relation between the reaction quotient and potential at any given temperature. Equation 8 can be used to study spontaneity of electrochemical reactions by comparing half-cell potential for redox pairs.

$$E_{cell} = E_{red} - E_{ox} \tag{9}$$

Where E_{cell}>0 V for a spontaneous reaction and E_{cell}<0 V if the reverse reaction is favoured. At equilibrium the cell potential is zero and E_{red} and E_{ox} are equal.

3.2.2 Phase stability diagrams

A useful tool for studying metals in aqueous solutions at different conditions are phase diagrams [38]. These diagrams are used extensively to study predominant species at equilibrium as a function of pH, electrochemical potential and ligand concentrations. Pourbaix diagrams (Eh-pH) show predominant species as a function of pH and potential and are especially useful for leaching since they can reveal favourable conditions for dissolving metals.

The diagrams are rooted in chemical equilibria between species based on Equations 2 and 8 and can thus only be used at equilibrium, making them unsuitable for very slow reactions. Equilibrium calculations also require accurate activity modelling at high ionic strength and Pourbaix diagrams should therefore only be used as a guideline for concentrated electrolytes. Moreover, tabulated equilibrium constants may also come with some uncertainties. Another limitation is that only dominant species are shown and no information about other likely complexes is given.

Software such as HSC Chemistry can be used to model thermodynamics of reactions and phase stability diagrams with the help of databases containing property information about different species [44]. Throughout this work, HSC Chemistry 10 was used to predict $\Delta G_r°$ values and draw phase diagrams.

3.3 Leaching

Leaching is the process of extracting a desired substance from a solid material into an aqueous phase. This requires the solid to be contacted with water and the metal to be converted into a soluble form, typically ionic, which is usually achieved by chemical reaction with an acid or base [38]. An example is the conversion of metallic Fe to Fe^{2+} with acid solutions:

$$Fe(s) + 2H^{+}(aq) \rightarrow Fe^{2+}(aq) + H_2(g)$$

For leaching to occur, reactants and products need to be transferred between the aqueous bulk and solid surface [38]. This takes place via diffusion of the reactant from the aqueous bulk to the solid-liquid boundary layer and diffusion to metal surface after which chemical reaction takes place. Products then need to diffuse back through the film and into the bulk. Because of the many steps involved, leaching kinetics are not exclusively controlled by reaction kinetics but can also be limited by mass transfer, and identifying the rate limiting step is critical for optimizing the leaching process.

A major rate limiting factor in the leaching process is passivation of the solid surface. Whilst this is usually desirable in corrosion chemistry, in hydrometallurgy it prevents chemical reactions since these occur exclusively at the surface [45]. Passivation can occur by formation of an insoluble layer on the surface such as noble metal or oxide layer e.g., chromium oxide in stainless steel, and adsorption of gases or organic corrosion inhibitors.

To quantify the effectiveness of a leaching process, it is common to determine the fraction of individual metals extracted from a material. Percentage extracted or leaching efficiency ($\%\mathrm{E}$) is defined as the ratio of mass of a specific substance extracted from a solid over original mass of the substance in the solid prior to leaching.

$$\%E = 100 \cdot \frac{C_M V_l}{m_s x_M} \tag{10}$$

Where C_M is the mass concentration of metal M in a volume V_l of leachate, m_s is the original solid mass and x_M the mass fraction of M in the solid. For selective leaching to be achieved, efficiencies of the desired metals should be high while keeping impurity efficiencies low.

3.3.1 pH-static leaching

Leaching of metals is usually highly pH dependent and selective leaching can in some cases be achieved by controlling the pH in a leaching process [46, 47]. Contrary to conventional leaching tests where solids are mixed with a concentrated lixiviant and left to react, pH-static leaching involves continuous dosing of reactants at the same rate as their consumption by chemical reactions. While requiring additional process control, major advantages of this technique are that leaching is done under milder conditions, can achieve high leaching selectivity and only uses the required amount of chemicals. This is key in developing a lean and flexible leaching process even when feed materials are highly heterogeneous.

3.4 Metal separation by precipitation

Metals dissolved in the leaching process usually need to be treated further to separate out impurities. One separation technique where impurities are resolidified and removed by solid liquid separation are precipitation processes. Two common precipitation processes are hydroxide precipitation and cementation, but e.g., formation of insoluble metal carbonates or metal-organic complexes are also possible.

3.4.1 Hydrolysis and metal hydroxide precipitation

Water molecules can dissociate spontaneously to form hydroxide and hydronium (hydrogen) ions according to the autoprotolysis reaction

$$2H_2O \rightleftharpoons OH^- + H_3O^+ \tag{11}$$

In pure water solutions, only a fraction of molecules is dissociated, and a general equilibrium can be stated as

$$K_w = \frac{a_{H_3O^+} a_{OH^-}}{a_{H_2O}^2} \approx [H_3O^+][OH^-] \tag{12}$$

Where $K_w=10^{-14}$ is the water dissociation constant. In strongly acidic solutions, Reaction 11 is shifted to form H_2O with very little OH^- is present. In basic solutions on the other hand, very little H_3O^+ is present due to this equilibrium.

Dissolved metal ions form weak bonds with water molecules to form a coordination sphere around the metal ion (hydration) [38]. Water in the coordination sphere can be protolyzed or replaced with a OH^- ion, resulting in formation of a metal-hydroxide complex

$$M^{v+} + nH_2O \rightleftharpoons M(OH)_n^{(v-n)+} + nH^+ \tag{13}$$

When v=n in Equation 13, an uncharged metal hydroxide complex is formed which can precipitate as a solid. Hydrolysis occurs stepwise with different hydrolysis constants K_n for each step

$$K_n = \frac{a_{M(OH)_n^{v-n}} a_{H^+}}{a_{M(OH)_{n-1}^{v-n+1}} a_{H_2O}} \approx \frac{[M(OH)_n^{v-n}][H^+]}{[M(OH)_{n-1}^{v-n+1}]} \tag{14}$$

The cumulative hydrolysis constant is defined as the product $\beta_n=K_1K_2\ldots K_n$. According to Equation 14, hydrolysis depends on the H^+ concentration and is as such highly pH dependent. A higher degree of hydrolysis can generally be expected in basic solutions according to the equilibrium in Equation 12. Since hydrolysis constants vary between metal ions and even between oxidation states, metal separation can be achieved by hydrolysing and precipitating specific ions. Incorporation of other metals into precipitated solids (co-precipitation) usually cannot be avoided and leads to some loss of wanted metals or impurities in recovered precipitates.

3.4.2 Cementation

Cementation is an electrochemical reaction which is driven by difference in reduction potential between a solid metal acting as both the anode and cathode, and a dissolved metal ion [38]. The general reaction mechanism can be written as

$$nM^{m+}(aq) + mN(s) \rightleftharpoons nM(s) + mN^{n+}(aq) \quad (15)$$

An exchange of electrons takes place on the solid metal surface where the more noble, metal M is reduced and precipitated while the less noble metal N is oxidized and dissolved. The cell potential for Equation 15 is determined by Equation 9, and a larger cell potential E_{cell} results in an increased driving force making cementation more feasible.

The different steps that influence kinetics are similar to those for leaching reactions with transport of the dissolved noble metal to the less noble metal surface, precipitation of the noble metal on the surface by electron exchange and transport of the less noble metal to the bulk. Cementation is usually a mass transport limited process and can thus mainly be influenced by altering hydrodynamics and boundary layer conditions of the system [38].

3.5 Experimental design

Design of experiments (DOE) is a method used for optimizing the number of experiments versus amount of data gained when investigating systems with multiple influencing factors [48]. In contrast to traditional one-factor-at-a-time tests where one factor is varied while others are kept constant, DOE can be used to study multiple factors and their interdependency simultaneously to save time and resources.

Experimental design is usually performed in several steps starting with selection of a suitable response variable (e.g., metal concentrations) for studying a system [48]. Critical factors influencing the response with experimental ranges then have to be determined which is usually done by literature study, modelling and preliminary testing. Generally, it is desirable to keep the number of investigated factors low and factors with a small influence should be held constant throughout experimentation.

Factorial designs and response surface modelling are often used in research and industry for process optimization [48]. These methodologies are based on simultaneously testing multiple variables, creating and evaluating different regression models and drawing response surfaces for graphically interpretation of optimal processing conditions. The experimental variance can be estimated by performing repeated experiments at the centre of the design and assumed to be valid in the whole experimental region instead of performing replicates at each experimental condition. When determining variance in this way, wide variable ranges may however be less suitable. Verification of regression models can be done with Analysis of Variance (ANOVA) and statistical of individual regression coefficients.

4 Materials and methods

Swarf samples were provided by SKF AB (A) and Husqvarna AB (B) and were generated in the grinding of low alloy steel roller bearings and chainsaw blades respectively. Alumina grinding wheels and semi-synthetic emulsion cutting fluids (A: Castrol, Hysol SL 35 XBB and B: Castrol, Hysol SL 36 XBB) were used in each grinding process. Emulsions were similar with a base of 25-50% mineral oil, amines, neutralized carboxylic acids and alcohols mixed in concentrations of 5-6% with water.

Sample B was received as filtered and sample A was received as filtered and briquetted. Briquettes of swarf were pulverized and mixed by hand or with the aid of a ceramic mortar and pestle and both samples were stored individually in sealed polypropylene containers to prevent oxidation.

4.1 Leaching setup

The standard reactor setup is given in Figure 4. Jacketed glass reactors vessels (200 and 1000 mL) were used for leaching. External heating was provided by flowing hot water in the outer layer. The reactor lid was fitted with holes for stirring, acid dosing and pH measurement. Before initiating leaching tests, the reactor was filled with water or iron chloride solution from previous tests, which was preheated to desired experimental temperature after which swarf was added and acid dosing was initiated. Aliquots of the slurry were taken with a syringe and were filtered using PES syringe filters for analysis of leachate metal concentrations.

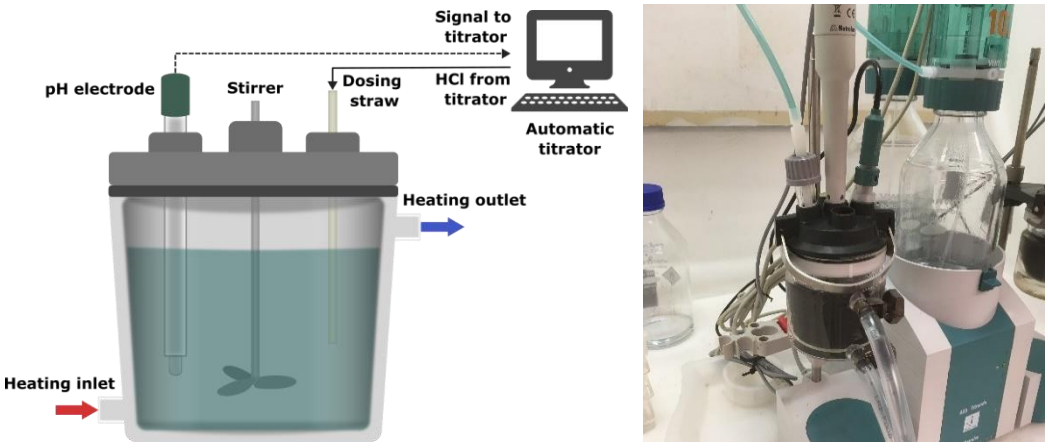

Figure 4: Schematic drawing of the leaching setup (left) and actual small scale leaching reactor (right) with external heating, stirring and pH control by acid dosing with an automatic titration device.

4.1.1 Automatic titration and pH control

Combined pH electrodes with Ag/AgCl reference and Pt1000 temperature sensors (Unitrode/Syntrode, Metrohm) were used to measure pH during leaching experiments. Electrodes were connected to an automatic titrator (Titrando 905, Metrohm) for adding varying concentration of HCl (ASC Reagent, 37%) to the reactor using a dosing device (Dosino 800, Metrohm) via a polypropylene straw with anti-diffusion tip. The acidity in a solution was

controlled by programming the titrator to dose hydrochloric acid whenever the pH exceeded the desired level. As acid was continuously consumed by reactions, slight fluctuations in the pH value were inevitable.

Temperature, ionic strength and other factors can influence the measurement of the hydrogen ion activity and hence estimation of pH [49]. To minimize the impact of temperature, calibration of the electrodes was done by measuring potentials of pH 7.00, 4.00 and 2.00 buffer solutions at the same temperature as experiments. Any variations in the condition of the electrode between experiments should also be accounted for in this way. Ionic strength, dielectric constants and ionic charge size can also influence hydrogen ion activity, however since metal ion concentrations varied during and between experiments, these factors were not accounted for.

4.1.2 Filtration and handling of leachate and solid residues

After leaching tests were completed, leachate filtered using a cellulose filter paper with a vacuum filtration setup. Filtrates were stabilized by addition of a few drops of concentrated hydrochloric acid before storage in sealed glass bottles to prevent oxidation of $FeCl_2$. Filter cakes were washed with 100 mL water and air dried >24 h in a fume hood and dry solids were weighed before storage in 50 mL polypropylene vials.

4.2 Liquid phase characterization

Inductively coupled plasma-optical emission spectroscopy (ICP-OES, Thermo Scientific iCAP Pro) was used to analyse metal concentrations in aqueous solutions. Calibration was done at the start of each session with prepared elemental standard solutions. Liquid samples were diluted with 0.5 M HNO_3 (Merck Suprapur, 69%) to bring metal concentrations within the calibration range. Low dilution factors were required to analyse metal impurities while high factors were required for measuring Fe.

Due to high $FeCl_2$ concentrations in impurity measurements, significant matrix effects which can disturb measurements were expected. This can be accounted for by having the same background in calibration solutions and samples. Two separate calibration solutions were created for Fe and impurities. For Fe a 1000 ppm elemental standard (Teknolab Sorbent AB) was diluted with 0.5 M HNO_3 to concentrations of 0.625-20 ppm. Impurity standards were prepared with the same method but were spiked with $FeCl_3$ (Iron(III)chloride reagent grade, 97%) to mimic expected Fe concentrations in the sample solutions.

4.3 Solid phase characterization

Qualitative analysis of solids was done using microscopy and X-ray diffraction and quantitative analysis was done using ICP-OES after digestion in aqua regia, X-ray fluorescence, carbon/sulphur analysis and Soxhlet extraction.

X-ray diffraction

Phase characterization was done using powder X-ray diffraction (XRD, Bruker D8 Discover). A Cu source with wavelength 1.5406 Å was used to analyse samples with 2Θ between 10° to 80° with increments of 0.04° and scan rate of 0.04°/s. Peak analysis was done by comparison with the JCPDS database in DIFFRAC.EVA software.

Aqua regia digestion and ICP-OES

Metal contents were analysed by digesting triplicates of 0.2-0.5 g of solids in 30 mL aqua regia (1:3 HNO_3:HCl) at 80°C for 2 h with regular swirling of the E-flask. After digestion, each solution was made up to 50 mL with Milli-Q water and aliquots were filtered, diluted in 0.1-0.5 M HNO_3 and analysed with ICP-OES.

X-ray fluorescence

Since some solids were usually left after aqua regia digestion, X-ray fluorescence (XRF) analysis was done as a complement and for comparison with ICP-OES results. An Axios Wavelength Dispersive XRF with Rh anode was used, with 2-4 g samples prepared in polypropylene containers with 6 μm film for radiation exposure in a He atmosphere. Iron and alloying elements were assumed to be metallic when analysing untreated swarf while leaching residues were analysed as oxides or hydroxides. Carbon, cutting oil ($C_{15}H_{32}NO$) and water contents were fixed based on previous fluid and water analysis when normalizing metal concentrations.

Total carbon analysis

Total carbon (TC) was analysed via combustion/IR analysis (LECO CS744). Approximately 0.1 g of solids were weighed and added to an alumina crucible before loading into the combustion chamber. Combustion was done at 1000°C to convert organic and inorganic carbon to CO_2 which was quantitively measured with NDIR spectroscopy.

Soxhlet extraction

Soxhlet extraction was used to estimate hydraulic and cutting fluid contents in grinding swarf. Approximately 20 g solids were added to a cellulose thimble and weighed. The thimble was placed in the extractor and washed with at least 5 refluxes with ethanol (Solveco analytical grade, 95%). Thimble and solids were then air dried and weighed to assess the mass loss after washing.

Dean-Stark moisture determination

Moisture contents of solids were determined with a Dean-Stark apparatus by mixing 20 g swarf with 250 g Toluene (anhydrous, 99.8%). Toluene forms an azeotrope with water which boils at a lower temperature than water or toluene individually. Since water is insoluble and heavier than toluene, it could be collected by the apparatus and weighed to assess the moisture content of solids in the toluene solution.

4.4 Experimental design and regression modelling

A 2^3 face centred cubic (FCC) experimental design as seen in Figure 5, with 4 centre point experiments was used to study the effects of temperature, pH and L/S ratio on leaching of metals. Levels for each factor are shown in Table 2 and were based on results from preliminary leaching tests, Eh-pH diagrams and limitations for pH control. Time was also considered as a factor but excluded from the experimental design after preliminary kinetics studies. Though this design lacks even variance prediction around the centre points due to distance variations to the centre, it was selected to avoid impractical conditions at the axial points [48].

Table 2: Factors used in the experimental design with their respective ranges.

Factor	Low (-1)	Mid (0)	High (+1)
Temperature (°C)	20	40	60
pH	2	3	4
L/S (mL/g)	50	35	20

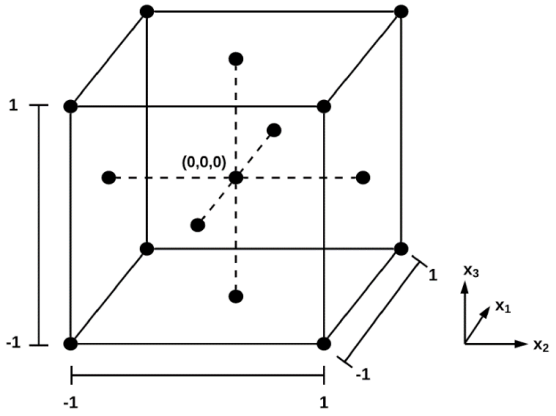

Figure 5: Face centred cubic (FCC) factorial design.

Temperatures above 80°C quickly degrade the electrode and accordingly a lower temperature of 60°C was selected. The Eh-pH diagrams for the Fe-Cl system showed that precipitation of Fe(III) is likely to occur already around pH 1 between 20-60°C (see Supporting material). On the other hand, Fe(II) was stable up to pH 6-7 but more sensitive to oxidation to Fe(III) at pH >5 due to formation of easily oxidizable $Fe(OH)^+$ and $Fe(OH)_2^0$ [50]. Regardless, accurate dosing was difficult over pH 4 and this was set as the upper limit. Chromium was regarded as the main impurity and was stable up to pH 1-1.5. As a result, separation of Fe and Cr could potentially be achieved and pH 2 was selected as the lower limit. An initial volume of 100 mL water was used in each test, and L/S was varied by adding different amounts of swarf. Low L/S caused difficulties with mixing in the smaller reactor and 5 g swarf (L/S=20 mL/g) was set as the upper limit.

Results from the experimental design were interpreted with regression modelling and response surface methodology. Statistical and graphical analysis was done with MATLAB based on DOE theory by Montgomery [48].

5 Results and discussion

5.1 Swarf characterization

Physically the grinding swarf appeared as a powder or fluff and microscopy images in Figure 6 show that it is made up of unevenly formed, interlocked shavings. Briquetted sample A featured a dense structure while B consisted of an open network of slightly larger shavings. The gleam of the swarf suggested that most of the steel was in metallic form. Alumina abrasives appeared as beige or blue specs scattered randomly in the shavings. Abrasives would occasionally fall out when lifting the fluff which can make representative sampling challenging. Abrasives are not metallurgically bonded but can often be found physically trapped within the complex steel network [15].

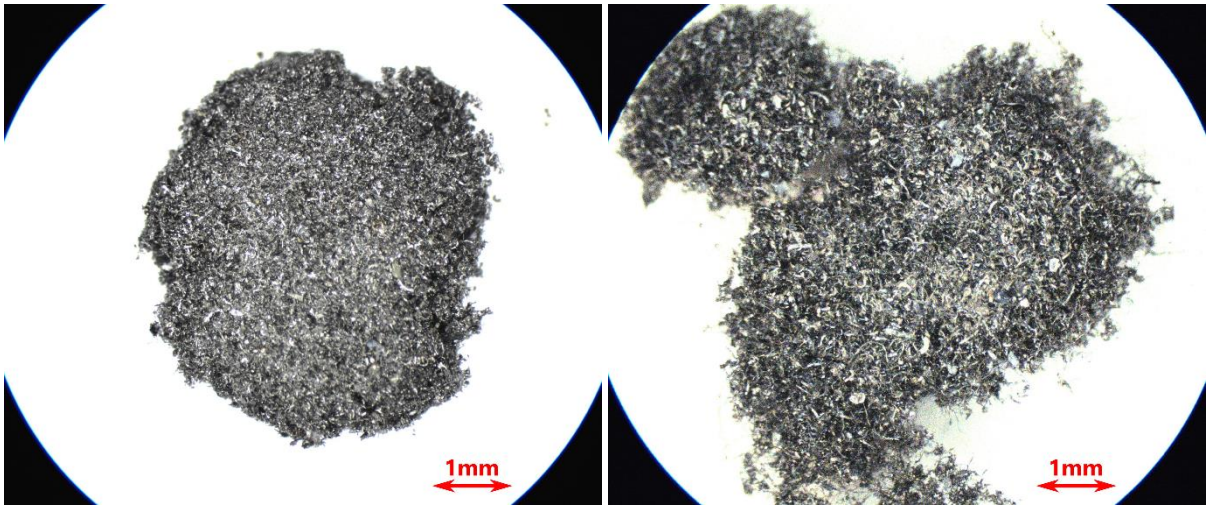

Figure 6: Microscopy images of grinding swarf A (left) and B (right).

5.1.1 Phase characterization

Phase analysis with XRD was performed to study crystalline structures of the steel fractions and characterize abrasives. Figure 7 shows that both samples contained mainly ferritic steel (α-Fe) with significant peak broadening at both ferrite peaks 44° and 65° due to incorporation of alloying elements in the lattice. Some differences between the steels can be observed with austenite (γ-Fe) peaks in A at 2Θ of 51° and 75°. Both samples appeared mostly unoxidized despite observing some local light brown discolorations in A.

Alumina (corundum) was identified to be the only abrasive type in each sample. Corundum peaks in B were barely visible compared with A which is either due to differences in abrasive contents or a result of non-representative sampling. Generally, abrasives are designed to have a high mechanical, chemical and thermal resistance and should be difficult to dissolve in dilute acid solutions.

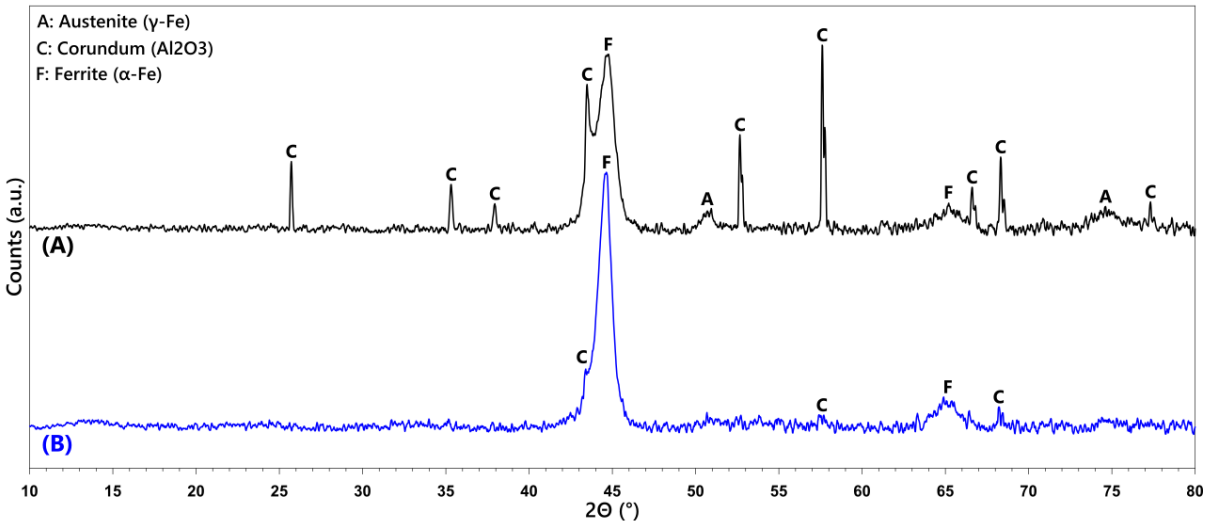

Figure 7: XRD analysis of swarf samples from grinding of bearings (A) and chainsaw blades (B).

5.1.2 Chemical composition

Chemical compositions of the grinding swarf are given in Table 3. Metal contents in the steel were determined with ICP-OES after dissolution in aqua regia and verified with XRF, while abrasives and were insoluble in aqua regia and quantified solely with XRF. Fluid contents were determined with Dean-Starke and Soxhlet extraction. The carbon content (TC) represents a total of both organic and inorganic carbon which were not distinguishable. Other components included O, H, S, P and alkali and alkaline earth metals (Na, K, Mg, Ca), and their quantities were calculated as the rest of 100 wt-% after summing steel, abrasives and cutting fluids contents.

Table 3: Chemical compositions of grinding swarf samples. Uncertainties for steel components and carbon were based on triplicate measurements while abrasive uncertainties came from intensity variations in single XRF measurements.

Steel			Abrasives, cutting fluids & other		
Element	**A (wt-%)**	**B (wt-%)**	**Component**	**A (wt-%)**	**B (wt-%)**
Fe	78.4 ± 0.8	68.4 ± 1.9	Al_2O_3	7.75 ± 0.08	3.1 ± 0.05
Cr	1.13 ± 0.01	0.41 ± <0.01	SiO_2	0.72 ± 0.03	0.61 ± <0.01
Mn	0.37 ± <0.01	0.23 ± <0.01	Cutting fluid	~6.2	~25.2
Ni	0.10 ± <0.01	0.64 ± <0.01	Water	~3.7	~19.5
Cu	0.10 ± <0.01	0.04 ± <0.01	Lubricant	~2.5	~5.7
Mo	0.09 ± <0.01	<LOD	TC	6.11 ± 0.17	2.45 ± 0.15
Al	0.04 ± <0.01	0.19 ± <0.01	Other	4.9	1.1
Co	0.01 ± <0.01	0.01 ± <0.01			

Similar alloying elements were found in both samples with higher levels of Cr and Mn in A and higher levels of Ni and Al in B. Sample A contained more Fe due to its low cutting fluid content and represented a more promising material for iron chloride production. Though reported standard deviations in Table 3 are small, large variations in steel and abrasives fractions may

occur between batches due to dressing of the grinding wheel. Abrasive contents in Table 3 confirm that A contained more Al_2O_3 which explains differences in peak height observed in XRD. Silicon was also detected in in each swarf which may either be present as Si in the steel or SiO_2 as binder material from the grinding wheel which were not distinguishable.

A summary of cutting fluid constituents based on safety data sheets (SDS) for Hysol SL 35 XBB and Hysol SL 36 XBB, is shown in Table 4. Due to the harsh conditions in the grinding process and aging of samples, degradation products of the original fluid components may also be present in the swarf.

Table 4: Constituents of the cutting fluids present in swarf samples A and B based on SDS.

Constituent	A (wt-%)	B (wt-%)	Function	Reference
Petroleum distillates	25-50	25-50	Lubricant	PubChem
Ethanolamine	≤13	≤8	Corrosion inhibitor, pH regulator	PubChem,[51]
Dicyclohexylamine	≤10	≤10	Corrosion inhibitor, lubricant	PubChem,[51]
Neodecanoic acid	-	≤10	Corrosion inhibitor, pH regulator	PubChem
(Z)-octadec-9-enol	≤5	-	Solvent, lubricant	PubChem
Methyldiethanolamine	≤5	≤5	Corrosion inhibitor, pH regulator	PubChem,[51]
Triethanolamine	≤5	≤10	Corrosion inhibitor, pH regulator	PubChem,[51]
Alcohols, C16-C18	≤3	-	Emulsifier	PubChem
Glycolic acid ethoxylate oleyl ether	≤3	-	Emulsifier	Sigma
Alkyl ether carboxylic acid	≤3	-	Emulsifier	Sigma
2-Octadec-9-enoxyethanol phosphoric acid	-	≤3	Solvent, emulsifier	PubChem
Oleic acid	-	≤3	Emulsifier	PubChem
Aminomethyl propanol	-	≤3	Emulsifier, lubricant	PubChem
5-Carboxy-4-hexyl-2-cyclohexene-1-octanoic acid	-	≤3	Corrosion inhibitor, surfactant	PubChem
Tolyltriazole sodium salt	≤0.3	≤0.3	Corrosion inhibitor	Sigma

Sample B contained around 25.2% cutting fluids of which 19.5% water, while A only contained around 6.2% with 3.7% water after briquetting. Though both manufacturers reported using 5-6 wt-% emulsions in water some drying may have occurred before taking samples from the production line. This partially explains the difference in water/organic ratios between samples but more importantly, (tramp) oils have been shown to be difficult to remove from the steel surface by pressing [25]. Water removal can therefore be assumed to be more efficient than removal of organics in the briquetting process.

Total carbon (TC) analysis contradicts the estimated cutting fluid contents with 6.11% carbon in A and only 2.45% in B. Carbon may be present in the steel, cutting fluid, tramp oils and binder materials and since inorganic and organic carbon were indistinguishable, it was difficult to determine the reason for differences in TC. Assuming that both steels had similar carbon contents, one explanation is that A contained more organic binder materials and tramp oils. This is reasonable since A contained more abrasives and had a faint oily smell after Soxhlet washing. Ethanol was able to dissolve Hysol SL 35 XBB completely based on solubility testing with pure emulsion but may have been less suitable for washing out non-polar hydraulic oils. Sample A also contained a larger quantity of unidentified substances which may among others include tramp oils or binders.

5.2 Leaching experiments and regression modelling

Sample A was used exclusively in investigation of leaching conditions. A 200 mL reactor vessel (D=6 cm) with a polypropylene stirrer (D=3 cm) operating at 1500-1800 rpm was used to study the effects of time, temperature, pH and L/S on leaching of metals from grinding swarf. Initially, water leaching tests were conducted to observe if anything could be leached without addition of acid. Thereafter, pH was controlled by dosing 5 M hydrochloric acid in all further tests.

5.2.1 Thermodynamical modelling of leaching reactions

Leaching reactions were first studied thermodynamically to predict what elements could be leached and whether leaching conditions were oxidizing or reductive. Two main feasible leaching mechanisms for Fe with hydrochloric acid were identified and are given in Equations 16 and 17, with $\Delta G_r°$=–44.0 kJ/mol and $\Delta G_r°$=–4.8 kJ/mol respectively.

$$Fe(s) + 2HCl(aq) \rightarrow FeCl_2(aq) + H_2(g) \quad (16)$$

$$Fe(s) + 3HCl(aq) \rightarrow FeCl_3(aq) + \frac{3}{2}H_2(g) \quad (17)$$

Where aqueous $FeCl_2$ is light blue and $FeCl_3$ is yellow to brown and mixtures of both tend to be somewhere between green, yellow and brown. In practice, the overall reaction can be assumed to occur via Equation 16 since the colour of the leachate was generally clear blue. In the presence of oxygen, Fe(II) can spontaneously oxidize to Fe(III) according to Equation 18 with $\Delta G_r°$=–330.8 kJ/mol.

$$FeCl_2(aq) + HCl(aq) + O_2(aq) \rightarrow FeCl_3(aq) + H_2O \quad (18)$$

This reaction was observed to be very slow, and any formed Fe(III) can be assumed to be rapidly reduced to Fe(II) in the presence of metallic Fe via Equation 19.

$$Fe(s) + 2FeCl_3(aq) \rightarrow 3FeCl_2(aq) \quad (19)$$

This reduction was relatively fast based on an immediate colour transition from green to blue of slightly oxidized iron solutions when mixed swarf. Bubbling of H_2 in the system may also have a reductive effect on Fe(III) according to standard reduction potentials:

$$Fe^{3+} + e^- \rightleftharpoons Fe^{2+} \qquad E° = +0.77\,V$$

$$Fe^{2+} + 2e^- \rightleftharpoons Fe \qquad E° = -0.44\,V$$

$$2H^+ + 2e^- \rightleftharpoons H_2 \qquad E° = 0\,V$$

This favours stability of Fe in the solution as Fe(II) is stable at higher pH than Fe(III) which can precipitate as FeO(OH) with dissolved oxygen or $Fe(OH)_3$ without oxygen at pH ≥3 [52].

Leaching mechanisms of common alloying elements were expected to follow reactions similar to Fe with formation of Cr(III), Mn(II) and Ni(II) by reactions with hydrochloric acid. An exception is Cu which is more noble with E°>0 and thus requires oxidizing conditions to be leached as Cu(II) according to Eh-pH diagrams. Due to the reducing conditions in the solution, there was little to no risk of forming highly undesirable Cr(VI).

5.2.2 Water leaching

Water leaching tests were performed at L/S=50 mL/g and 20, 40 and 80°C for 2 h. A pH increase from 7 to 8-9 was noted after adding swarf in each case, likely because of amines in the cutting fluid which act as Lewis bases. Some difficulty in mixing swarf with water was initially observed due to the fluffy and hydrophobic nature of the material, however, after a short time of mixing larger agglomerates broke up and mixing was greatly improved.

No metals were leached from the swarf at any temperature. At 80°C the solution took on a slightly yellow hue which could have been caused by oxidation of the steel surface, but no dissolved Fe was detected. In each test, the turbidity of the water increased and gained a milky colour over time which signified that cutting fluids were re-emulsified. This meant that release of cutting fluids into the leachate was also expected during leaching.

5.2.3 Preliminary leaching kinetics studies

Leaching kinetics were studied to determine how fast metals were dissolved at different pH levels. Since the goal was to maximize leaching of Fe and Cr was considered most critical to separate due to its high content in the swarf, these elements were focused on when determining leaching rates.

Both Fe and Cr reached a steady %E after 3 h at pH 2 according to Figure 8. At pH 4, the Fe concentration never reached a plateau even after 6 h while efficiencies for Cr levelled out after 3 h. Based on these results, Cr concentrations could generally be considered to reach steady levels after 3 h at pH ≤4, and this time was selected for all further tests. Since Fe leaching was significantly slower at low temperatures and high pH, some influence of time was expected at such conditions in the experimental design.

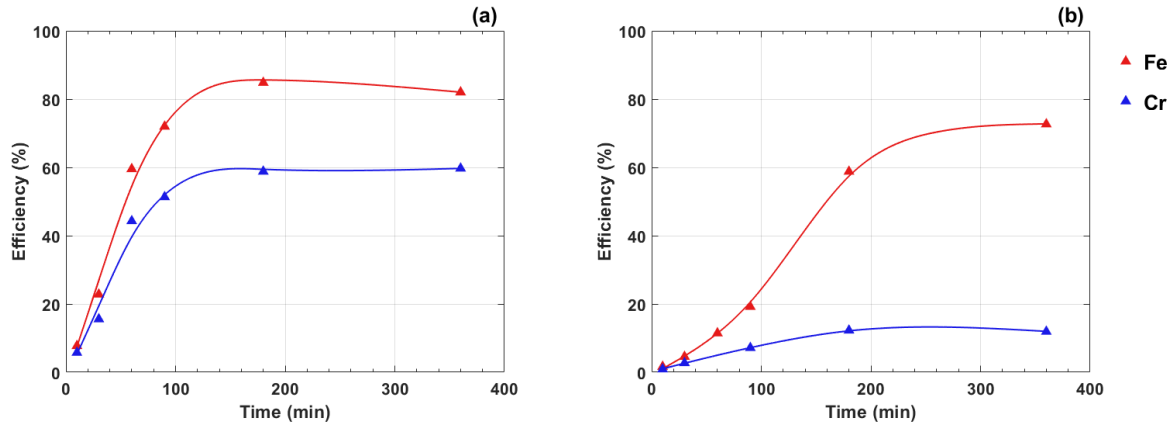

Figure 8: Leaching kinetics for Fe and Cr at 20°C, L/S=50 mL/g and (a) pH 2 and (b) pH 4

5.2.4 Experimental design and regression modelling

Optimal conditions for selective leaching of Fe in the predetermined temperature, pH and L/S ranges in Table 2 were investigated with DOE, and %E for Fe, Cr, Mn and Ni are given at each tested experimental condition in Table 5. Other alloying elements were also investigated but found in too low concentrations for predictive regression modelling. Best separation of Fe and Cr was achieved at pH 4 and 60°C and close to complete dissolution of Fe was possible at pH 2 and 60°C according to Table 5.

Table 5: Experimental design for leaching tests with leaching efficiency responses.

Random order	Standard order	Coded variables			Real variables			Response (%E)			
		x_1	x_2	x_3	T (°C)	pH	L/S (mL/g)	Fe	Cr	Mn	Ni
11	1	-1	-1	-1	20	2	50	82	50	70	47
18	2	1	-1	-1	60	2	50	100	56	85	100
13	3	-1	1	-1	20	4	50	33	2	28	21
1	4	1	1	-1	60	4	50	87	<1	71	66
10	5	-1	-1	1	20	2	20	83	47	67	37
2	6	1	-1	1	60	2	20	100	57	86	87
8	7	-1	1	1	20	4	20	15	6	14	6
12	8	1	1	1	60	4	20	58	1	48	20
3	9	0	0	0	40	3	35	95	35	77	80
6	10	0	0	0	40	3	35	96	45	77	84
4	11	0	0	0	40	3	35	93	42	76	77
14	12	0	0	0	40	3	35	86	38	72	76
15	13	-1	0	0	20	3	35	58	33	51	25
7	14	1	0	0	60	3	35	96	21	80	100
17	15	0	-1	0	40	2	35	93	54	78	94
5	16	0	1	0	40	4	35	67	5	55	44
9	17	0	0	-1	40	3	50	96	45	79	100
16	18	0	0	1	40	3	20	88	36	72	49

To better interpret the results in Table 5, regression and response surface modelling needed to be done. A second order regression model with two-way and three-way interactions was fitted to the experimental responses using the least square method. Final regression models with statistically significant variables only are given in Equations 20-23.

$$\%E_{Fe} = 91.5 + 17.1x_1 - 19.8x_2 - 5.4x_3 + 7.6x_1x_2 - 5.9x_2x_3 - 13.1x_1^2 - 10.2x_2^2 \quad (20)$$

$$\%E_{Mn} = 75.0 + 14.1x_1 - 17.0x_2 - 4.6x_3 + 5.4x_1x_2 - 4.4x_2x_3 - 9.2x_1^2 - 8.3x_2^2 \quad (21)$$

$$\%E_{Ni} = 78.6 + 23.7x_1 - 20.7x_3 - 13.5x_3 - 18.2x_1^2 \quad (22)$$

$$\%E_{Cr} = 37.8 - 25.0x_2 - 8.9x_1^2 \quad (23)$$

The models were evaluated and optimized with ANOVA, coefficients of determination and *t*-testing of individual regression coefficients. Table 6 shows ANOVA for regression Equations 20-23 and indicates that each model was significant with $F>F_{crit}$. Testing for Lack of fit (LOF) was also done to determine how well the selected regression model fitted the data in each case and shows that there was no significant LOF for Fe, Mn and Cr. For Ni however, $F_{LOF}<F_{crit}$ and it could be concluded that the variables included in the model did not entirely reflect trends in the data. To minimize LOF, $x_1x_2x_3$ and x_3^2 terms were eliminated from the Ni model but since LOF was still significant, inclusion of higher order terms (x_i^3) or interactions may be required. This was not investigated since the meaning of third order terms and interactions can be difficult to interpret physically and the model in Equation 22 was deemed sufficient.

Table 6: ANOVA for regression models in the leaching optimization DOE.

Response (%E)	Source	Sum of squares	Degrees of freedom	Mean square	*F*-value	Critical *F*-value
Fe	Regression	9635	10	963	32.80	3.64
	Error	206	7	29	-	-
	Lack of fit	138	4	35	1.53	9.12
	Pure error	68	3	23	-	-
	Total	9840	17	-	-	-
Mn	Regression	6470	10	647	47.96	3.64
	Error	94	7	13	-	-
	Lack of fit	77	4	19	3.38	9.12
	Pure error	17	3	6	-	-
	Total	6565	17	-	-	-
Ni	Regression	15456	8	1932	16.25	3.23
	Error	1070	9	119	-	-
	Lack of fit	1030	6	172	12.66	8.94
	Pure error	41	3	14	-	-
	Total	16527	17	-	-	-
Cr	Regression	6887	10	689	21.95	3.64
	Error	220	7	31	-	-
	Lack of fit	166	4	41	2.31	9.12
	Pure error	54	3	18	-	-
	Total	7106	17	-	-	-

Pareto diagrams showing significance of individual regression coefficients are shown in Figure 9. Absolute standardized effects higher than the given *t*-statistic represent significant variables which were included in in Equations 20-23. Note that $x_1x_2x_3$ and x_3^2 were eliminated from the Ni model. A general conclusion can be drawn that pH had a dominant influence on leaching efficiency in each case and was almost the sole contribution for leaching of Cr.

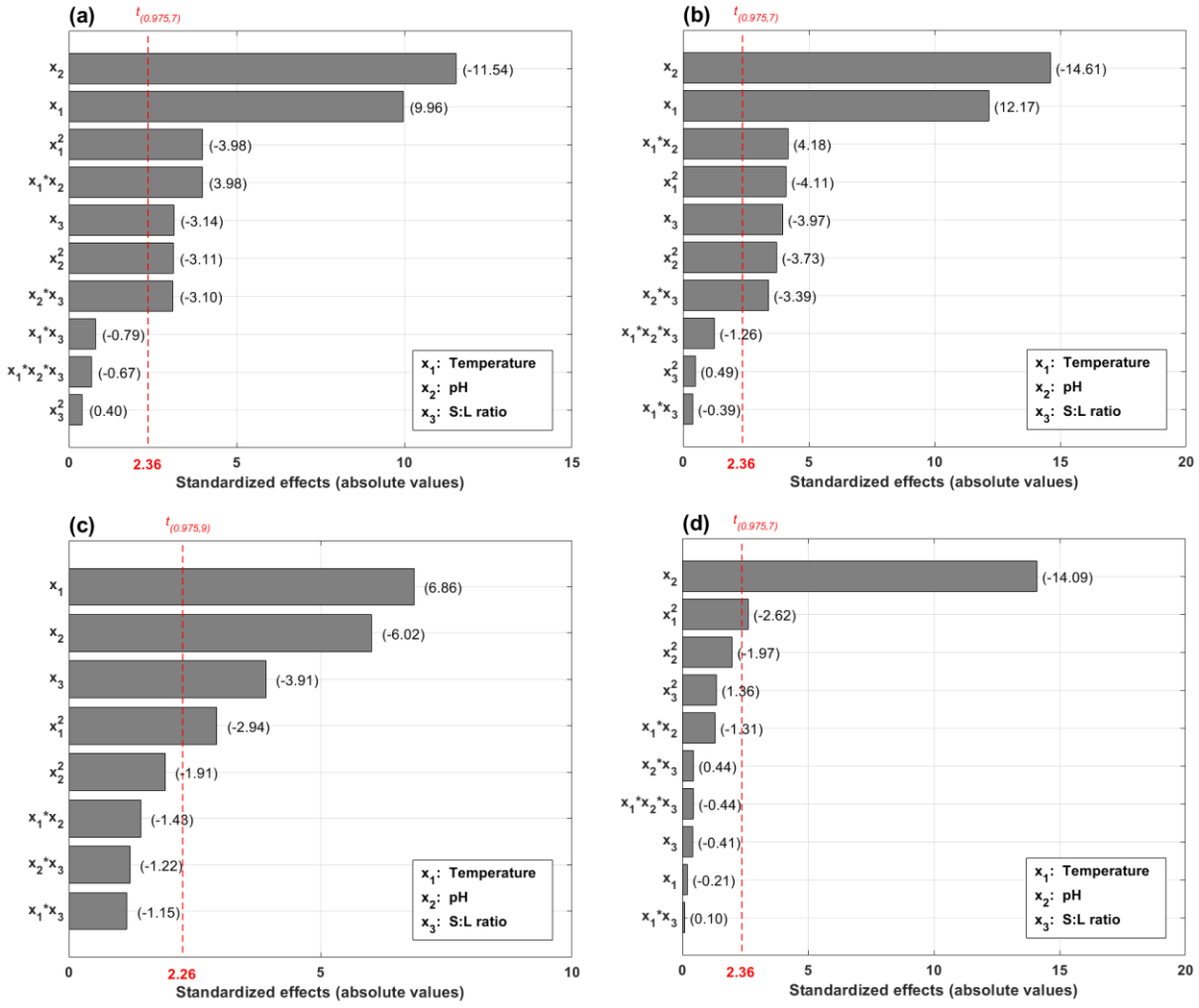

Figure 9: Pareto diagrams with standardized effects for individual regression variables for models of Fe (a), Mn (b), Ni (c) and Cr (d). Dashed red lines indicate critical *t*-statistics and standardized effects above the given *t*-value are significant.

Figure 10 shows goodness of fit evaluations with adjusted coefficients of determination. Predicted data for Fe and Mn followed experimental data well and standard deviations σ_{Fe}=5.42% and σ_{Mn}=3.67% explained any variations. Some spread was observed in the data for Cr and Ni which was mostly explained by standard deviations of σ_{Cr}=5.60% and σ_{Ni}=10.91%, but for Ni this can also be attributed to LOF in the regression model.

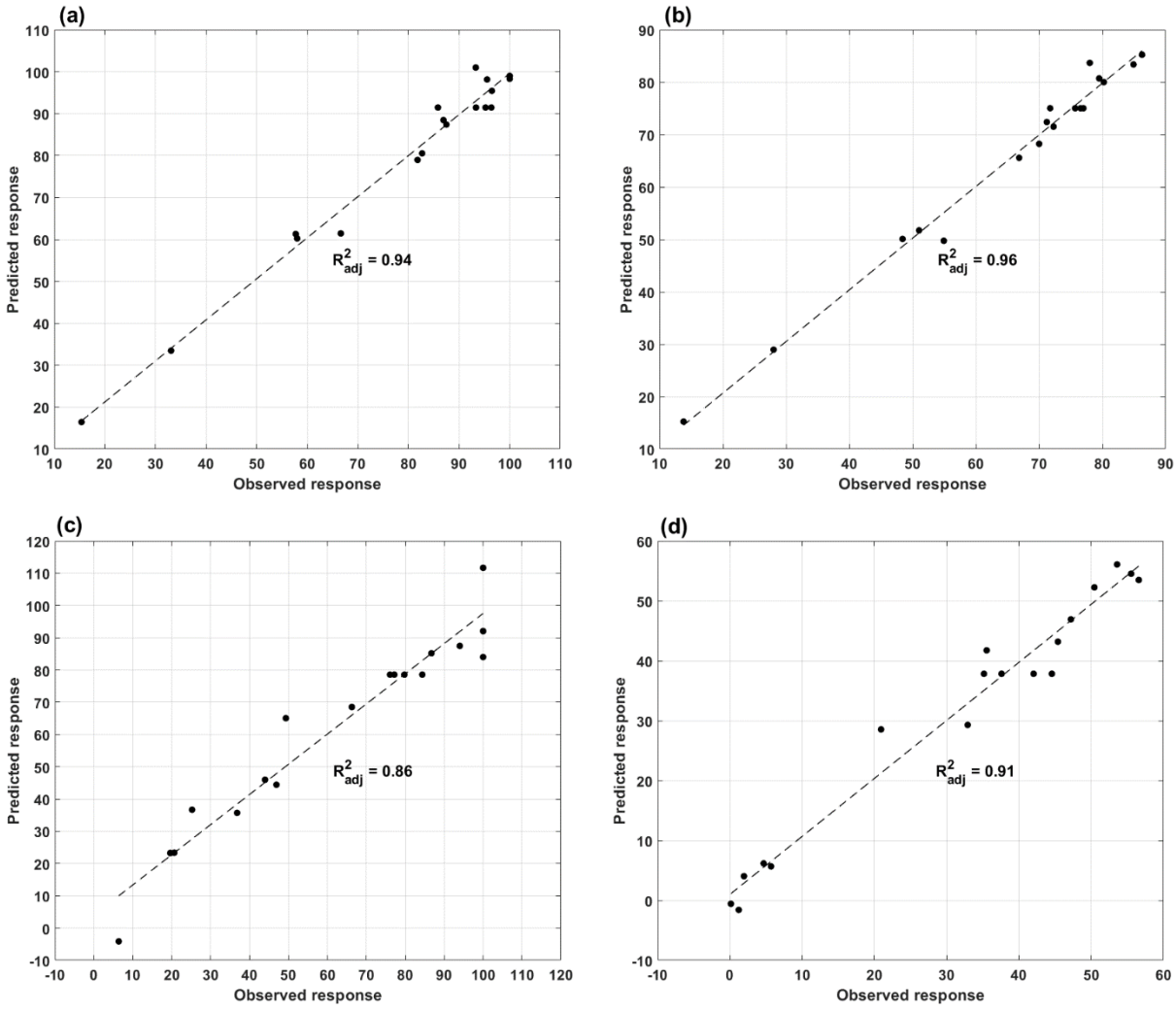

Figure 10: Experimentally observed responses versus responses predicted by regression models of Fe (a), Mn (b), Ni (c) and Cr (d). Goodness of fit is indicated with adjusted coefficients of determination.

To conclude, regression models for Fe and Mn were highly significant and fitted experimental data well. Since these models were very similar, comparable leaching behaviours and no opportunity for selective leaching is expected between Fe and Mn. The Cr model was reliable but with a slightly higher relative standard deviation (RSD) and thus lower predictability. Leaching of Cr was dominated by pH and selective leaching between Fe and Cr was possible. The model for Ni should be used with some precaution due to a high RSD. Selectivity between Fe and Ni is not obvious and needed to be investigated more closely with response surfaces.

5.2.5 Response surfaces and leaching optimization

Visual interpretation of regression models was done by plotting responses for two variables (temperature and pH) within the experimental range while keeping one (L/S ratio) constant at 20, 35 or 50 mL/g. Contour plots of 3D response surfaces are given in Figure 11. Leaching of Cr was independent of x_3 and is valid at all L/S ratios. An important thing to point out is that stable conditions were not achieved for Fe at 20°C and pH 4 within 3 h according to Figure 8 and higher efficiencies could be reached given more time.

In response surfaces for Fe, it can be seen that close to complete dissolution of Fe can generally be achieved at combinations of temperatures >40°C and pH below 3. Maximum efficiencies are shifted towards lower pH values with decreasing L/S ratios which is an effect

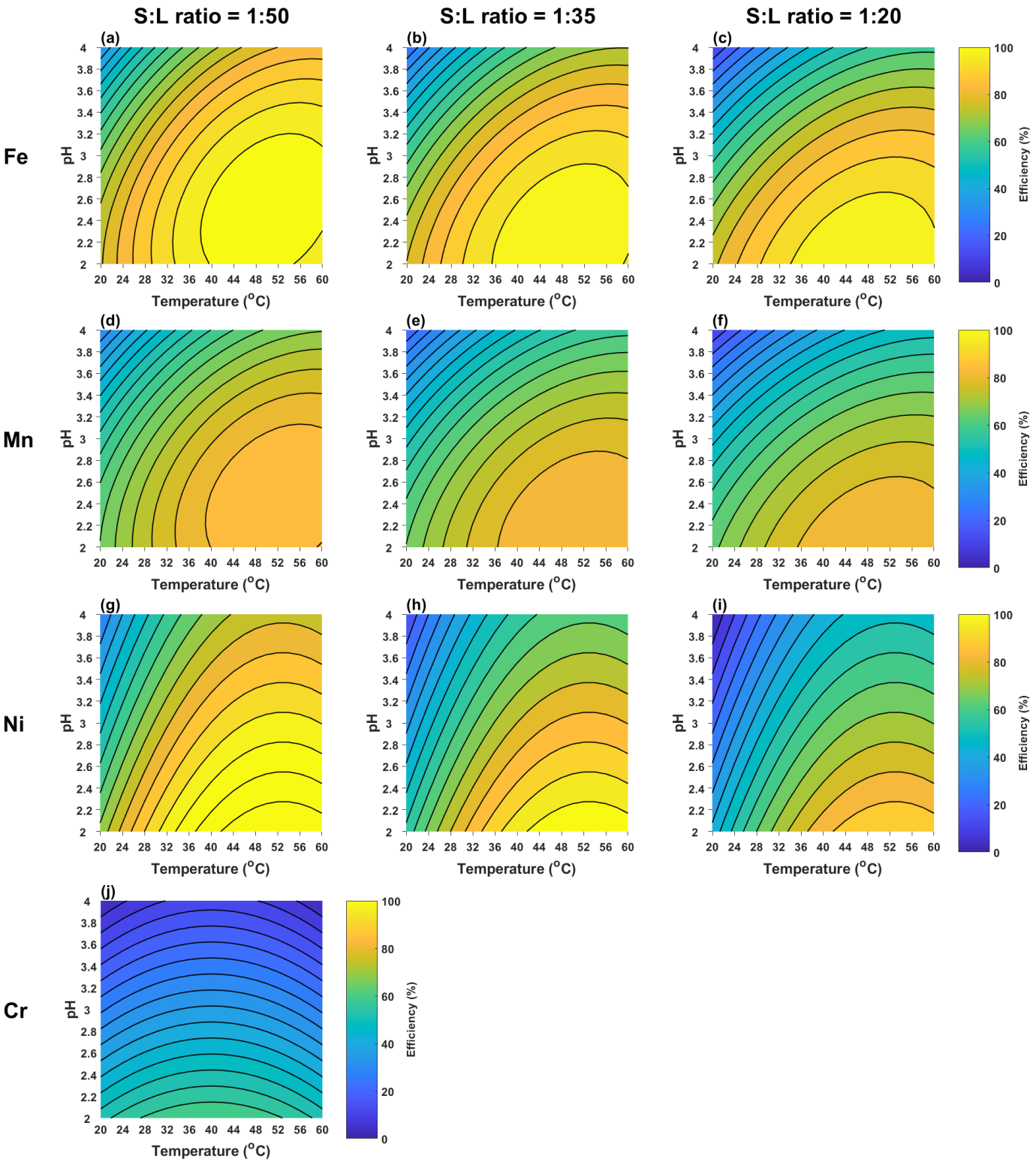

Figure 11: Response surfaces for regression models of Fe (a-c), Mn (d-f), Ni (g-i) and Cr (j) as functions of temperature and pH while keeping L/S ratios at constant levels of 20, 35 and 50 mL/g. Leaching of Cr was independent of L/S and is valid at all ratios.

of slower kinetics due to lower availability of acid per metal in the system. An interesting thing to note is that %E above 80% were not achieved at 20°C regardless of pH. The same observation was made in the kinetics test which suggests that temperatures >20°C are required to dissolve some part of the steel.

Comparison of Figure 11a-c with d-f reveals the similarities in leaching behaviour between Fe and Mn with almost identical dependencies on temperature, pH and L/S ratio. Despite Mn generally being slightly less leachable, selective leaching of Fe over Mn is impossible within the investigated conditions. This is in line with thermodynamics which showed that leaching was spontaneous, and that Fe^{2+} and Mn^{2+} were stable throughout the experimental range.

Looking at response surfaces for Ni in Figure 11g-i, some differences from Fe can be noted. Primarily, L/S ratio seems to have a greater impact on Ni which can be explained by parallel cementation while leaching according to Equation 24.

$$Fe(s) + Ni^{2+}(aq) \rightleftarrows Fe^{2+}(aq) + Ni(s) \quad (24)$$

The reduction potential of Ni(II)/Ni (E°=–0.26 V) is higher than Fe(II)/Fe (E°=–0.44 V) and thus there is a driving force to adsorb dissolved Ni onto the swarf surface. At low L/S ratios when more swarf is present, a higher surface area is available for cementation. Besides L/S ratio, leaching of Ni was influenced by the temperature to a greater extent than Fe and the dissolution could be minimized by operating at low temperatures.

Leaching of Cr shown in Figure 11j, was different from other metals and less Cr was generally dissolved. Since Cr was the main metal impurity, separation from Fe was critical and could be achieved by keeping the temperature at 20 or 60°C and pH 4. More Fe extraction was observed at high temperatures and thus 60°C was preferrable. There was also some indication when comparing experiment 3 & 4 and 7 & 8 in Table 5, that Cr was extracted to a lesser extent at high temperatures. This trend was confirmed by Eh-pH diagrams which showed a lower soluble Cr(III) stability at elevated temperatures. There were two possible reasons why Cr was seemingly less leachable: either metallic Cr and Cr_2O_3 from oxidation of Cr by air, were more difficult to dissolve, or Cr was continuously leached and precipitated by hydrolysis as $Cr(OH)_3$ via Equation 25.

$$Cr^{3+}(aq) + 3H_2O \rightleftarrows Cr(OH)_3(s) + 3H^+ \quad (25)$$

To summarize, optimal leaching conditions for dissolving Fe were identified to be combinations of temperatures above 40°C and pH below 3 while L/S ratio had an effect on kinetics but no observed effect on extractability. Selective leaching could but achieved for Cr and Ni but not for Mn. Leaching of Cr was minimized by operating at 60°C and pH 4 while Ni leaching was possibly counteracted by favourable conditions for cementation at L/S=20 mL/g.

5.3 Development of a recycling process for $FeCl_2$ production

Continued efforts focused on outlining a recycling process for producing industrial grade iron chloride solutions. Several improvements of the leaching process were required to bring the $FeCl_2$ closer to commercial standards. Firstly, according to regression modelling only 60% leaching efficiency was achieved for Fe within 3 h at conditions optimal for metal separation. This generates more solid residue which can be a problem in secondary waste management. Therefore, a way of extracting all Fe while maintaining Cr separation was needed. Secondly, the iron content of the final solution was only around 0.5 M $FeCl_2$ (2.5 wt-% Fe(II)). This was far from industrial grade 3.5 M $FeCl_3$ (13.8 wt-% Fe(III)) and demanded an efficient way of concentrating Fe. Separation of Ni from Fe was also insufficient so far. The selected approach was to tackle these problems in order, starting with optimizing Fe and Cr separation.

In further experiments, a 1 L round bottom leaching reactor (D=10 cm) with polypropylene coated stirrer (D=7 cm) operating at 300 rpm was used with an initial aqueous volume of 300 mL. Both swarf samples A and B were investigated for comparison of filtration and briquetting pretreatment methods on metal leachability.

5.3.1 Impurity precipitation by hydrolysis

Some indication was given that dissolved Cr would hydrolyse and precipitate at elevated pH allowing separation from $FeCl_2$ by filtration and metal stability as a function of pH was investigated. Sample A was first leached at 60°C, pH 2 and L/S=10 mL/g which in accordance with regression modelling should result in steady metal concentrations with complete dissolution of Fe. After leaching, an additional 1-2 g of swarf was added to the slurry to consume excess acid and raise the pH to a higher level which was then maintained for 30 minutes before sampling. This process was repeated until pH 4.5 when acid consumption by halted due to slow metal dissolution. Graphs showing metal concentrations as a function of pH are given in Figure 12. Raising pH with a strong base such as NaOH was feasible up to pH 2 but at higher levels Fe was precipitated by hydrolysis without achieving any change in pH.

According to Figure 12, metal concentrations were constant up to pH 3.5. In the range on pH 3.5-4.5, Cr, Mo and Al started precipitating and Cr contents were reduced from 650 ppm to 2.3 ppm. The most likely mechanism of precipitation was by hydrolysis as amorphous $Cr(OH)_3$ as proposed in Equation 25, rather than oxides (Cr_2O_3, CrO(OH), etc.) since leaching conditions were relatively anoxic due to constant H_2 bubbling.

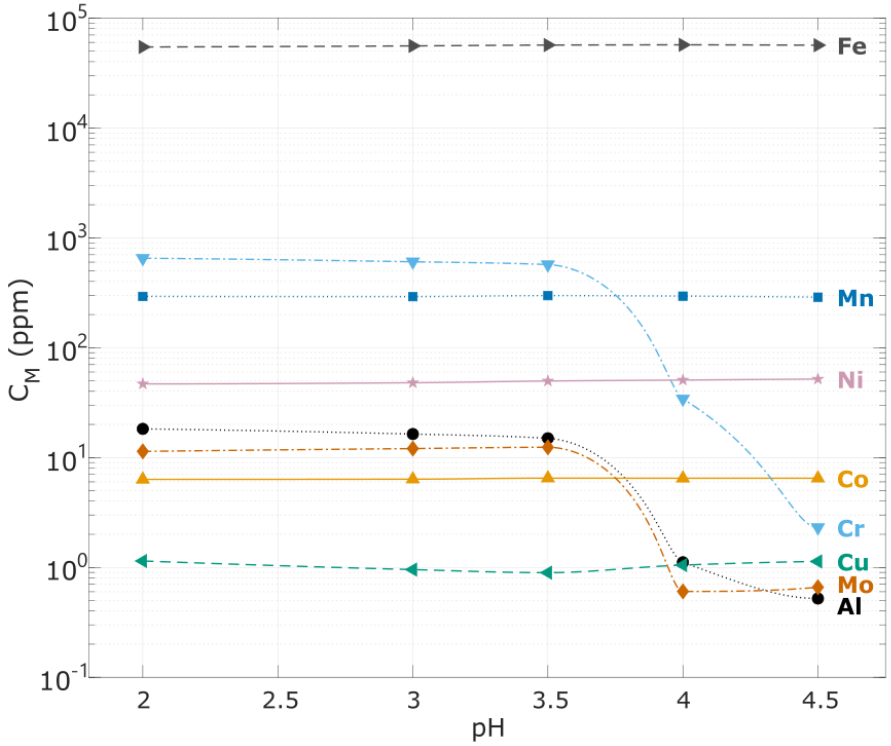

Figure 12: Metal concentrations in a leachate when gradually lowering the acidity level from pH 2 to pH 4.5. Conditions: T=60°C, L/S=10.

The simultaneous precipitation of Al and Mo may also be explained by hydrolysis. Precipitation of Al(III) as $Al(OH)_3$ has been shown to be feasible between pH 4-6 at 25°C while Mo should have a low solubility in dilute acids due to $MoO_3 \cdot H_2O$ formation [53, 54]. Since Al and Mo removal coincided with Cr, this could also indicate some kind of coprecipitation mechanism. This was however outside the scope of this study since Al and Mo are not regarded as problematic to the iron chloride product.

Another important observation from Figure 12 is that $FeCl_2$ concentration remained at 0.9 M throughout the study and no buildup of brown iron oxides was observed in the solution. This confirms that iron is kept as stable Fe(II) which allows efficient separation from Cr, Al and Mo with minimal Fe losses. No visible impact on Mn, Ni and Co can be seen despite additions of swarf in each step which would allow for Ni and Co cementation [55, 56]. The concentration of Cu remained around 1 ppm as was predicted thermodynamically, and any dissolved Cu could easily have been cemented onto Fe due a great difference in standard reduction potential [57].

5.3.2 Two-step consecutive leaching and precipitation for chromium separation

Results from the precipitation study were tested for both samples A and B by consecutively leaching at pH 2 and precipitating at pH 4. Leaching efficiencies for different metals are shown in Figure 13. As predicted, around 90% Fe was leached after 3 h for A and after raising the pH, any dissolved Al, Cr and Mo precipitated yielding an iron chloride solution with Mn, Co and Ni as main impurities.

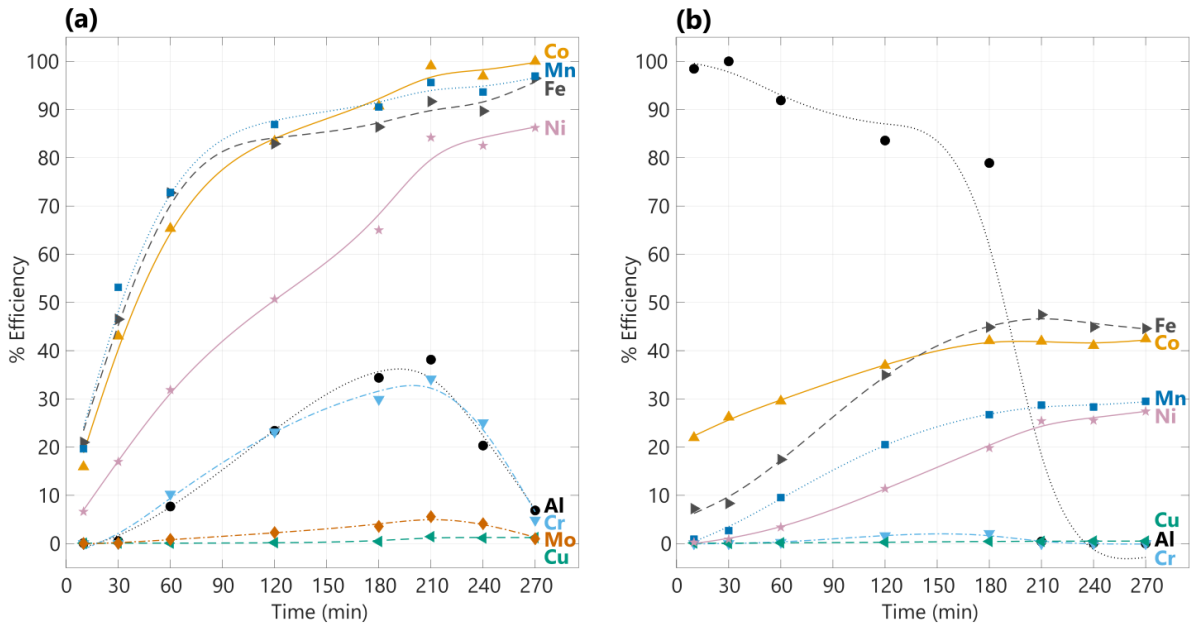

Figure 13: Leaching efficiencies for different metals in steel swarf samples A (a) and B (b) in a two-step consecutive leaching at pH 2-2.5 for 3 h and precipitation at pH 4 for 1 h. Initially, 60 g swarf was leached, and an additional 5 g was added after 180 minutes. Conditions: T=60°C, L/S=10 mL/g.

For sample B in Figure 13b, only 45% Fe was extracted after leaching. Likewise, %E for Co, Mn and Ni were also low which indicates that the steel was only partially dissolved. No Cr was also dissolved at any stage in the process which is explained by the fact that Cr was electroplated onto the chainsaw blades prior to grinding. Since Cr is easily oxidized by air, most Cr in B was present as Cr_2O_3 which has a higher resistance to acids than the metallic Cr in sample A. Another noteworthy difference is the behaviour of Al in Figure 13b which started off at 100%. This Al was not part of the steel but was rather present as microscopic (<45µm) abrasive particles which passed the syringe filters when preparing ICP-OES samples. In the first 180 minutes, the Al concentration decreased by dilution and during precipitation abrasive particles were likely aggregated by flocculation.

Comparison of XRD patterns of untreated swarf and leaching residues of sample A in Figure 14, show that both the ferrite and the austenite peaks had completely disappeared while the relative intensity of the corundum peaks had increased after leaching. The main residue from the steel fraction was cementite which has a higher C content and was likely more difficult to dissolve by protection of Fe by insoluble carbon atoms. Some FeO(OH) can also be seen which was formed when air drying the filter cake. Initially the cake was black but after 24 h, the colour changed to light brown typical for FeO(OH). No peaks for crystalline Cr_2O_3, CrO(OH) or similar could be detected which confirms that Cr was indeed precipitated as amorphous $Cr(OH)_3$.

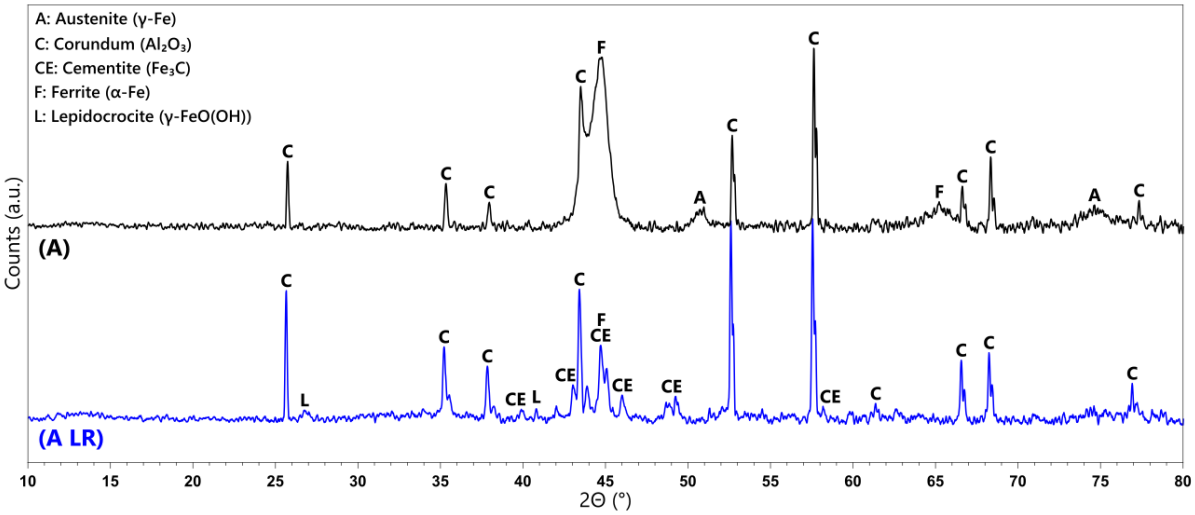

Figure 14: XRD patterns of sample A and residues (LR) after the two-step process with sample A.

Looking at patterns for sample B in Figure 15, it becomes clear that much of the ferrite remained intact after leaching, contrary to what was observed for sample A. Although dried filter cakes had a similar brown colour, this was likely just a thin oxide layer on top of a main ferrite body revealed by XRD. Unlike residues of sample A which were a thick sludge, leaching residues of swarf B still had the characteristic shape and texture of grinding swarf which shows that the steel shavings were largely intact. Leaching was therefore far less effective for sample B and the steel surface was passivated in some way.

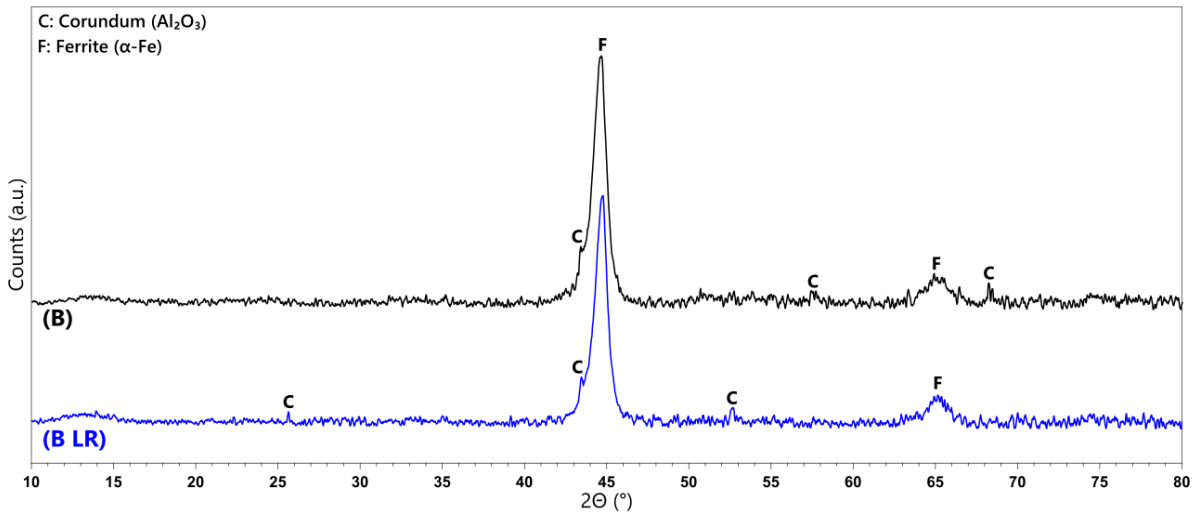

Figure 15: XRD patterns of sample A and residues (LR) after the two-step process with sample B.

Since morphologies of both samples were similar and Cr and Ni contents were too low to inhibit corrosion, self-passivation of the steel was unlikely [45]. Leaching residues also looked indifferent from untreated swarf and formation of a protective iron oxide layer was not observed until after drying the filter cake. Passivation by H_2 bubble formation and adsorption on the steel surface can also limit mass transfer of hydrochloric acid and leaching products but this is also improbable since no such behaviour was observed for A and swarf was mixed well with the aqueous media facilitating release of bubbles. The main difference between

samples was in cutting fluids and organic substances most likely played a critical role in passivation of the steel surface.

5.3.3 Cutting fluids in the leaching and precipitation process

Both cutting fluids were semi-synthetic emulsions with comparable constituents, however the cumulative quantity of inherent corrosion inhibitors such as amines and carboxylic acids was 33.3% in sample A and 46.3% in B according to Table 4. The protection mechanism of these substances varies but usually relies on formation of a hydrophobic film by bonding of e.g., amines with the metal surface [45, 58]. This separates the steel surface from aqueous solutions and can thereby prevent leaching. Another similar passivating effect can be expected from demulsification of lubricant oils during leaching.

When mixing swarf with water, the turbidity of the slurry increased and gained a milky colour. This was due to the re-emulsification of oils and within the first 60 minutes of leaching, the solution remained turbid. However, once metal concentrations started to increase the solution consistently became transparent and any emulsified oil seemed to have disappeared after filtration as seen in Figure 16. This was caused by several factors that lead to flocculation and coagulation of colloidal oil micelles [59, 60].

Figure 16: Hysol SL 35 XBB (6%) in water (left), swarf B mixed with water (centre) and filtered leachate (right).

Emulsified oils and other small particles are held in suspension by a repulsive electrical double layer with relative charge difference known as zeta potential (ζ-potential), which prevents them from nearing other similarly charged particles. When ions are introduced in the suspension medium, the thickness of the double layer and ζ-potential are minimized, and the oil is able to flocculate or coagulate to form larger droplets [59].

Demulsification of cutting fluids is therefore achieved by introducing an acid or salt to increase the ionic strength [59, 61]. Another contribution comes from hydrolysis of metal ions which is often the main destabilizing effect of coagulants [62]. Coagulation is also facilitated by high temperatures and mixing which promote mass transfer and increase the number of droplet-droplet collisions [59]. All these conditions were present in the recycling process and oil demulsification can be expected to be highly effective. Formation of a secondary phase was however barely discernible in most experiments which is either due to low oil contents of the swarf, or flocculation of coagulated oil by solids [62]. The latter is probable since no secondary phase or turbidity was observed in filtrates which means that any oil remained with solids in the filter cake. The flocculated oil could therefore in theory also form a hydrophobic layer on the steel during leaching, similarly to the inherent corrosion inhibitors.

The large volume of cutting fluid left in swarf B was presumably the main reason for lower leaching efficiencies. Initially when the ratio of metals to lubricant was high, leaching proceeded as normal, however, as more steel was dissolved this ratio decreased and the relative concentration of inhibitors and flocculated oil could have made dissolution more difficult [58]. It can therefore be concluded that further separation of cutting fluids by briquetting or centrifugation of swarf after filtration is necessary for optimal leaching.

5.3.4 Concentration of the iron chloride solution

Due to the poor results from sample B, efforts to concentrate an $FeCl_2$ solution were done only with sample A. Several techniques can be applied in concentrating metals in a solution including lowering the L/S and increasing acid concentration in leaching, recirculating leachate, evaporation of solvent and solvent extraction. Since the objective was to keep the process as energy and cost efficient as possible, low L/S (5 mL/g), high acid concentrations (37% HCl) and leachate recirculation were tested to avoid adding additional processing steps.

Recirculation was simulated by processing three swarf samples in steps (R0, R1 and R2), where initial aqueous phase was 300 mL filtrate from the previous step and R0 started with water. Leaching and precipitation were performed as described in Section 5.3.2 in each step. Metal concentrations, pH and total acid volumes added were measured in each stage and are given in Figure 17.

Leaching and precipitation proceeded as observed previously in R0 according to Figure 17a with a final concentration of 2.0 M $FeCl_2$. A slight decrease in Al, Cr and Mo can already be seen after 60 min due to the large fluctuations in pH. After adding 5 g of swarf for precipitation and $FeCl_2$ stabilization, Al and Cr contents were reduced to levels below the LOD for ICP-OES.

In R1 a concentration of 3.3 M $FeCl_2$ was reached, and leaching and precipitation behaviours were similar to R0 with Ni as a main exception. Concentrations of Ni decreased in the first 60 minutes and then increased until more swarf was added. After precipitation, concentrations were lower than filtrate from R0. A similar pattern was observed for R2 and was closely correlated to the macroscopic leaching behaviour of the swarf and cementation of Ni.

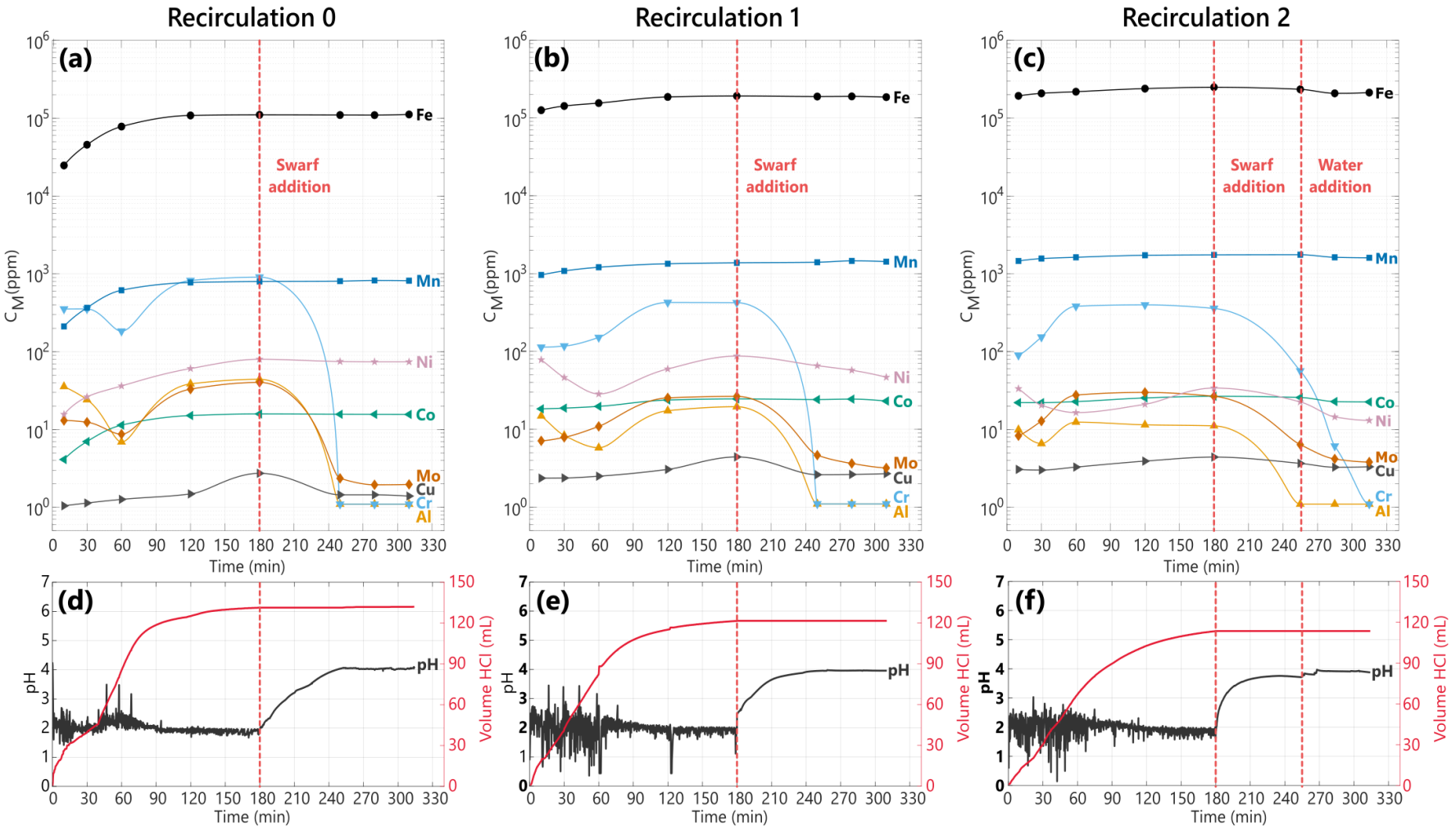

Figure 17: Metal concentrations during processing of swarf A by leaching and precipitation with reuse of leachate for 0 (a), 1 (b) and 2 (c) recirculations (denoted R). R0 started with 300 mL water while R1 started with 300 mL filtrate from R0, and R2 with 300 mL filtrate from R1. Development of pH and volumes HCl added in R0 (d), R1 (e) and R2 (f) are shown below each figure. Swarf was added for acid neutralization in all cases while water was only added in R2 to raise pH due to insufficient neutralization by the added swarf. Conditions: T=60°C, L/S=5 mL/g.

Solids were initially well mixed with the aqueous phase until acid addition started which caused swarf to be lifted by H_2 bubbles. This formed a metallic foam which remained on the liquid surface for the first 60-90 minutes of leaching as seen in Figure 18. Small amounts of swarf were occasionally pulled from the foam into the vortex and provided the solution with metallic Fe for Ni cementation. Towards the end of leaching, little metallic Fe was left, and Ni was redissolved due to a lack of competition for H^+ but with a fresh addition of swarf and lower acid concentration during precipitation, Ni was cemented again.

Figure 18: Leaching slurry after 60-90 minutes with a swarf foam on the liquid surface (left), and 180 minutes after disintegration of the cake (right).

Concentrations reached 4.5 M $FeCl_2$ at the end of leaching in R2 and blue $FeCl_2$ salt started forming on the reactor walls indicating that the solution was close to saturation. In theory, the saturation limit for $FeCl_2$ at 20°C is around 5.4 M with solubility increasing with temperature and no crystals should thus have been formed in the solution itself [63]. Another notable difference between R1 and R2 was that the Ni concentration was further reduced, and Co content remained constant at around 25 ppm throughout testing. This shows a correlation between $FeCl_2$ concentration and cementation which is discussed in detail in Section 5.3.5.

After adding swarf for precipitation in R2, pH initially changed relatively fast but then halted at 3.7 and started to decrease slightly. This was likely due to an early onset of Cr(III) hydrolysis which released H^+ into the solution and according to Figure 17c, the Cr concentration was indeed reduced from 360 to 55 ppm between sampling at 180 and 255 minutes. However, since the goal was to reach pH 4, 50 mL water (25 mL at 256 min and 25 mL at 265 min) was added in an attempt to reduce the acid concentration. Though Cr was successfully reduced to

very low concentrations in this manner, $FeCl_2$ was also diluted to 3.8 M which was undesirable. Acid consumption by metallic Fe was seemingly less inefficient at 4.5 M $FeCl_2$ and another method for acid neutralisation without introducing foreign substances may be required. One option could be addition of carbonates according to Equation 26.

$$FeCO_3(s) + 2HCl(aq) \rightleftarrows FeCl_2(aq) + CO_2(g) + H_2O \quad (26)$$

A final interesting observation is that the pH and at which Cr(III) precipitates seems to be independent of $FeCl_2$ concentration. This implies that formation chloride complexes such as $CrCl^{2+}$ and $CrCl^{+}$, has little effect on the formation of $Cr(OH)_3$.

The overall impact of recirculation on %E of Fe, and metal concentrations in filtrates of R0, R1 and R2 can be seen in Figure 19. Leaching of Fe seems to be slightly slower in R1 and R2 which can be expected since the system is closer to equilibrium conditions and may also explain the difficulty with modifying pH, although the difference is marginal and not reliable without replicates. Regardless, close to complete dissolution of Fe was achieved in each case. Figure 19 also shows that Fe and Mn concentrations increased similarly due to their identical leaching behaviour while relative concentrations of Ni and Co decreased.

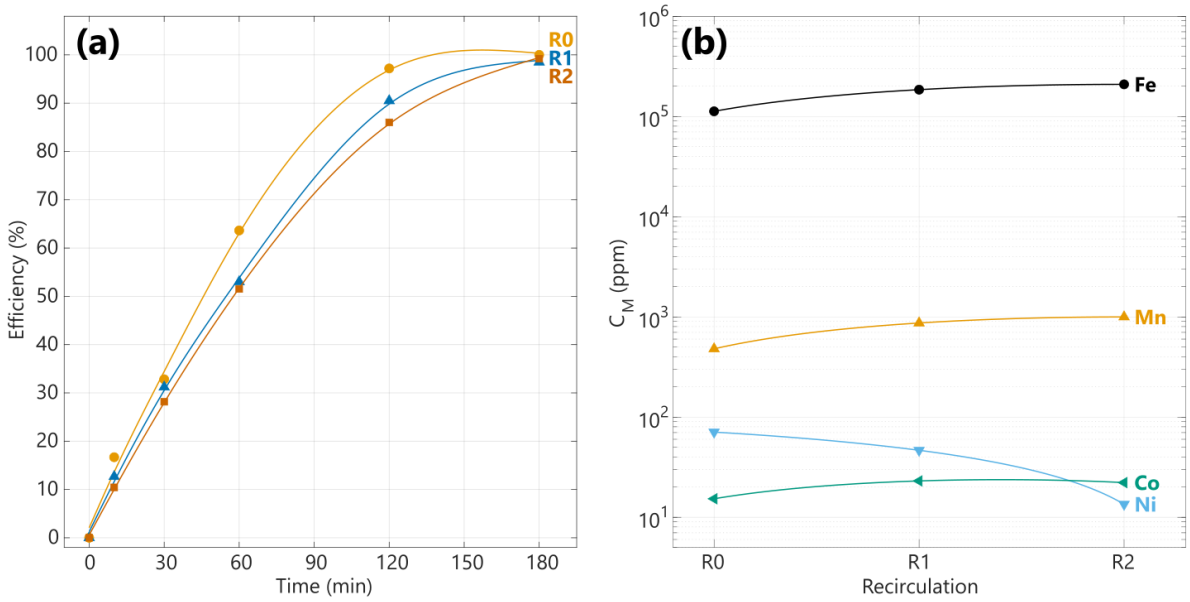

Figure 19: Leaching efficiencies for Fe in R0, R1 and R2 (a) and metal concentrations in filtrates after R0, R1 and R2 (b).

5.3.5 Cementation of nickel and cobalt

As evident from Figure 19, Ni cementation was more efficient at high $FeCl_2$ concentrations. The trend for Co was similar in the respect that the ratio of Co to Fe decreased from 136 mg/kg in R0, 125 mg/kg in R1 to 106 mg/kg in R2. This phenomenon has been observed previously for Ni and Co in different Cl^-, NO_3^- and SO_4^{2-} systems and shown to be most efficient in Cl^- systems [55, 56, 64, 65]. The process is most likely controlled by mass transport through the boundary layer and adsorption on the metal surface [38], although the exact function of

anions is not fully understood and explanations on both a macroscopic and molecular level have been suggested.

Macroscopically, Cl^- has been shown to clean metal surfaces from oxides and result in more favourable dendrite formation compared with other anions [55]. This can give a better surface for metal adsorption. Due to the quantity and complex shape of the swarf, large Fe surfaces should however already have been available for Ni and Co deposition in R0 as well as R1 and R2, and molecular interactions with Cl^- may provide better insight into the cementation mechanism. Two theories for Ni deposition and reduction via Ni^{2+} and a $NiCl^+$ complex have been proposed [66, 67].

Electrowinning studies by Jinxing suggested that only reduction of a Ni^{2+} specie was possible and $NiCl^+$ formation at high Cl^- concentrations inhibited deposition [67]. Positive effects of Cl^- on Ni deposition were explained by adsorption of Cl^- on the cathode surface which could make it easier for positively charged Ni ions to approach the metal surface.

Winand on the other hand proposed that cementation is possible either by reduction of Ni^{2+} or $NiCl^+$ [66]. In the proposed mechanism, reduction of Ni(II) involves two steps given in Equations 27 and 28, with an adsorbed Ni(I) intermediate. The first Ni(II)/Ni(I) step may involve side-chain reactions and is dependent on the Cl^- concentration, while the second Ni(I)/Ni step is independent of Cl^-.

$$NiCl^+(aq) + e^- \rightleftharpoons NiCl_{ads} \tag{27}$$

$$NiCl_{ads} + e^- \rightleftharpoons Ni(s) + Cl^-(aq) \tag{28}$$

It was observed by Hurlen that the first Ni(II)/Ni(I) step in Equation 27 was significantly faster for $NiCl^+$ than an analogue mechanism for Ni^{2+} which may lead to increased cementation rates with more Cl^- [68]. Hurlen also suggested that electrical double layer contributions by adsorbed Cl^- were small, contrarily to Jinxing's investigation.

Although rate limitations by chemical reactions are unlikely, it is still of interest to study chemical equilibria for cementation reactions to determine if these can affect the deposition. The reaction quotient for Ni^{2+} is given by Equation 29 and an analogue can be formulated for $NiCl^+$ with activity of Cl^- in the numerator.

$$Q = \frac{a_{Fe^{2+}} a_{Ni}}{a_{Fe} a_{Ni^{2+}}} \approx \frac{a_{Fe^{2+}}}{a_{Ni^{2+}}} \tag{29}$$

Relating this to the Nerst Equation (8), an expression for the electrochemical driving force is obtained in Equation 30.

$$E_{cell} = E^o_{cell} - \frac{RT}{nF} \ln Q = E^o_{cell} - \frac{RT}{nF} \ln \frac{a_{Fe^{2+}}}{a_{Ni^{2+}}} \tag{30}$$

Based on $FeCl_2$ concentrations in filtrates, the ionic strength increased from 6.0 M in R0, 10.0 M in R1 to 11.2 M in R2 which is outside the scope for reliable activity coefficient modelling,

but some general arguments can still be made. Primarily, cementation can be assumed to be less feasible at high Fe^{2+} and low Ni^{2+} activities and, disregarding activity coefficients, high Fe^{2+} and low Ni^{2+} concentrations. This is contrary to what was observed in Figure 19b and there seem to be no chemical equilibrium limitations despite increasing Fe(II)/Ni(II) ratios. This may be explained by large equilibrium constants for the cementation reaction [55], but also by chlorination of Fe(II) according to Equation 31 with formation constants K_1 and K_2 for the respective steps.

$$Fe^{2+} + Cl^- \rightleftharpoons FeCl^+ + Cl^- \rightleftharpoons FeCl_2^0 \quad (31)$$

Speciation diagrams were made with formation constants evaluated at zero ionic strength to give an indication of possible Fe, Ni and Co species and are shown in Figure 20 with K_i taken from the LLNL database (Fe: K_1=-0.16, K_2=-2.45, Ni: K_1=-0.99, K_2=-3.74, Co: K_1=0.15, K_2=-3.59) [69].

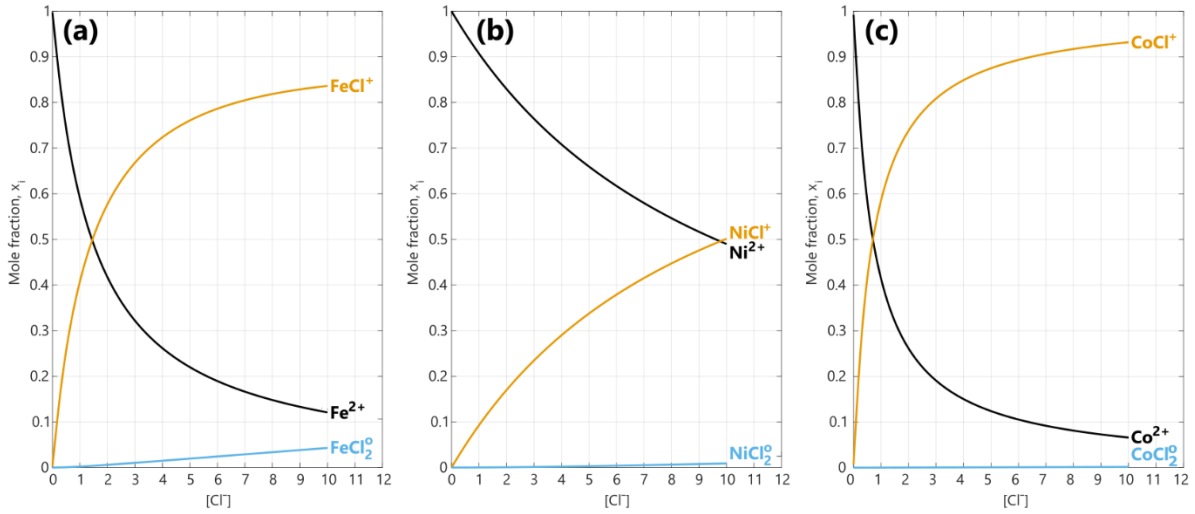

Figure 20: Speciation diagrams for Fe (a), Ni (b) and Co (c) in chloride media based on formation constants (K_i) from the LLNL database [69], evaluated at zero ionic strength.

At high Cl^- concentrations, $FeCl^+$ and Ni^{2+} dominate since Ni has a lower affinity for Cl^- and much of the Cl^- is complexed with Fe. This lowers the activity of free Fe^{2+} and hence increases the electrochemical driving force E_{cell} in Equation 30. Increased activity coefficients and reduction potentials for Ni(II) have been reported previously in chloride systems which confirms this theory [66, 67]. Winand reported reduction potentials as high as E=–0.058 V for Ni(II)/Ni in 4.5 M Cl^- systems with a small decrease for Fe(II)/Fe to E=–0.46 V at 30°C. This not only increases E_{cell} but also makes it more difficult for Ni to be redissolved by H^+. Chemical equilibria should therefore not limit but rather favour Ni cementation.

In terms of nobility, Co is comparable to Ni and cementation mechanisms similar to Ni(II) have been suggested for Co(II) [66]. Since Co has an even higher affinity for Cl^- than Fe as shown in Figure 20, cementation of Co should be more effective than Ni according to theories by Winand and Hurlen, but the opposite was observed in Figure 19. This supports the theory that cementation in fact occurs via uncomplexed Ni^{2+} and Co^{2+} species and is facilitated by

electrical double layer effects from adsorbed Cl^-. However, this may also simply indicate that the cementation mechanisms are different for Ni(II) and Co(II).

To conclude, cementation reactions were facilitated by Cl^- via good metal surface cleaning and dendrite formation. Other contributing effects from Cl^- adsorption on the steel surface or alternative cementation mechanisms via formation of Ni and Co complexes were also probable but less conclusive. Any cemented impurities should be more difficult to redissolve due to a shift in reduction potentials. Other undesirable impurities in coagulants such as Hg, Pb, Sn and Cd have higher E° than Fe(II)/Fe and could potentially also be removed from the solution by cementation [70, 71].

5.4 Final products and process design

Industrial grade $FeCl_3$ solutions for drinking water purification are classified into Type 1, 2 and 3 purity grades which set the limits for trace metal impurities. A comparison of the $FeCl_2$ solution obtained in R2 with $FeCl_3$ standard EN 888:2004 is given in Table 7.

Table 7: Metal concentrations in the $FeCl_2$ product after R2 and comparison with type 1-3 commercial grade $FeCl_3$ impurity levels for drinking water applications (EN 888:2004).

Element	Concentration (mg/L)	Purity (mg/kg Fe)	Type 1* (mg/kg Fe)	Type 2* (mg/kg Fe)	Type 3* (mg/kg Fe)
Fe	210 000	-	-	-	-
Mn	998	4773	5 000	10 000	20 000
Co	22	106	n/a	n/a	n/a
Ni	14	65	60	350	500
Cr	5	26	50	350	500
Cu	4	20	n/a	n/a	n/a
Mo	4	17	n/a	n/a	n/a
Al	<1	<1	n/a	n/a	n/a

*40 wt-% $FeCl_3$ solution basis

A first observation is that the Fe content of 210 g/L corresponds to a 34.4 wt-% $FeCl_2$ solution while commercial solutions are 40 wt-% $FeCl_3$ (195 g/L Fe). This means that the product both needs to be oxidized and concentrated further. Nevertheless, the solution is close to Type 1 based on trace metals with Mn, Co and Ni as main impurities and even lower Ni and Co concentrations can be expected according to trends in Figure 19, when concentrating the solution further.

Despite visually appearing free from cutting fluids (see Figure 16c) the $FeCl_2$ had a rank, fishy odour which among others likely stems from water soluble amines. Synthetic cutting fluids may therefore be less suitable for production of iron chloride solutions compared to straight oils or emulsions with fewer water-soluble components. Either way, a method for deodorisation and organic carbon removal is necessary for the $FeCl_2$ product and several

promising alternatives have been identified which combine oxidation of Fe(II), organic carbon to CO_2 and potentially Mn oxidation and precipitation as MnO_2. Hydrogen peroxide (H_2O_2) is a strong oxidant which can oxidize $FeCl_2$ and remove cutting fluid residues via Fenton oxidation where Fe(II) acts as a catalyst in formation of ·OH radicals which decompose organic substances [12]. Ozone combined with UV has a similar effect on organics. Chemical oxidants generally have a poor sustainability profile, and a more environmentally friendly oxidation route may be possible with electrochemistry [72–74].

A comparison of leaching residue XRD patterns from R0 and R2 is shown in Figure 21. As seen previously, residues from the steel consisted mainly of high carbon cementite which was insoluble in the leaching process. Abrasives also remained intact during leaching and can be observed in both residues R0 and R2. The main difference between the residues is that the relative size between corundum and lepidocrocite peaks has shifted with more FeO(OH) in R2. This is related to the difference in $FeCl_2$ solution concentrations between R0 and R2. Since part of the aqueous phase was absorbed by the filter cake, more $FeCl_2$ was left in solids after filtration and Fe can proceed to oxidize to lepidocrocite and magnetite when air dried [75]. Evidence of $FeCl_3$ in R2 is also given by two peaks at 2Θ 33.3° and 69.9°.

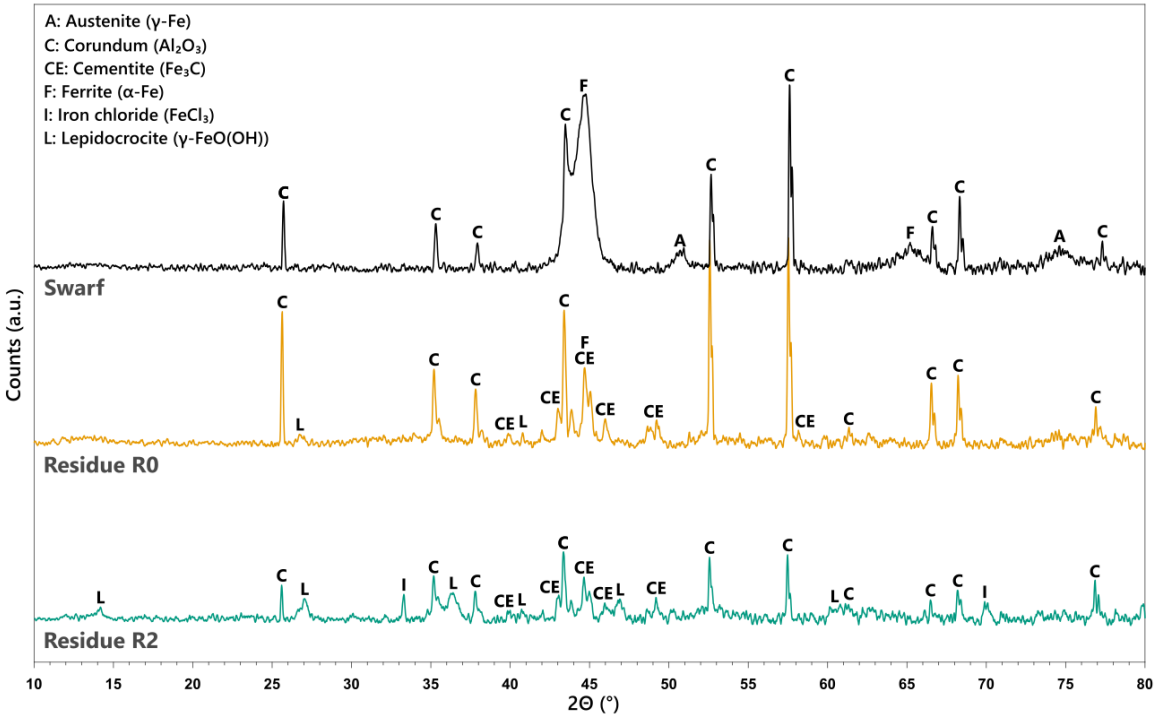

Figure 21: XRD analysis of swarf A and leaching residues from R0 and R2.

The volume of gangue material such as Al_2O_3 and $Cr(OH)_3$ in the filtration may have a high influence on the final mass of solid residues. Removing abrasives prior to leaching can potentially minimize secondary waste generation and $FeCl_2$ recovery. In all leaching experiments with sample A, ~0.5 g dry sludge/g input swarf was left after filtration.

Chemical analysis of dried sludge was also done to investigate possible applications for the solid residue and list of components based on XRD, XRF and TOC analysis is given in Table 1. Since ratios of Fe, FeO(OH) and $FeCl_3$ could not be distinguished, all iron was assumed to be FeO(OH). Inorganic and organic carbon were balanced as C and $C_{15}H_{32}ON$ based on TOC measurement.

Table 8: Chemical composition of leaching residue sludge with metal impurities from XRF and carbon from TOC analysis.

Compound	**R0 (wt-%)**	**R1 (wt-%)**	**R2 (wt-%)**
FeO(OH)	52.90 ± 0.30	69.40 ± 0.30	67.80 ± 0.30
$Cr(OH)_3$	12.10 ± 0.10	7.50 ± 0.01	8.32 ± 0.09
Al_2O_3	10.10 ± 0.10	3.28 ± 0.05	5.42 ± 0.07
SiO_2	3.36 ± 0.05	1.66 ± 0.04	2.22 ± 0.04
MoO_3	2.08 ± 0.04	1.76 ± 0.04	1.46 ± 0.04
Cl	2.20 ± 0.04	2.94 ± 0.05	3.06 ± 0.05
Cu	0.46 ± 0.03	0.63 ± 0.03	0.43 ± 0.02
Ni	0.70 ± 0.03	0.44 ± 0.03	0.42 ± 0.02
MnO	0.37 ± 0.02	0.35 ± 0.02	0.43 ± 0.02
TOC	11.57 ± 0.12	8.60 ± 0.24	8.31 ± 0.18
C	2.00	2.00	2.00
Organic ($C_{15}H_{32}ON$)	12.10	9.50	8.00
Other	0.86	0.52	0.48

Results in Table 8 confirm that the ratio of FeO(OH) to other solids increased with concentration of the $FeCl_2$ solution. The difference between R1 and R2 is small since final solution concentration did not differ much. What is noteworthy is the high quantity of alloying elements such as Cr, Mo and C which are concentrated in the leaching process. This can make the sludge an attractive raw material for production of alloy steel. Commercial recycling processes such as the Oxycup, DK and Scandust process are available for producing steel from steelmaking dusts and sludges and can potentially also be suitable for recycling leaching residues. These thermal processes require a source of carbon for metal oxides reduction which is already present in high quantities in the sludge according to Table 8. Recycling of the secondary material is critical both from an economic and environmental perspective since it would otherwise require deposition in landfills for hazardous waste due to its high oil content.

5.4.1 Process flowsheet

From results obtained so far, it is possible to outline a recycling process for producing high purity $FeCl_2$ and H_2 from (grinding) swarf and a proposed flowsheet is given in Figure 22. Based on leaching and precipitation studies, it is preferable to operate at ≥60°C throughout the process to ensure fast reaction rates, efficient hydrolysis of Cr and cementation of Ni and Co, and high solubility of $FeCl_2$ [55, 56, 63]. During leaching, hydrochloric acid may be provided by dosing stoichiometric amounts at a constant rate or by operating at constant pH ≤2 to achieve

complete dissolution of Fe. In the precipitation step, pH 4-4.5 is preferred to ensure complete Cr removal and the pH may be adjusted by adding more swarf and a non-hydroxide based neutralizing agent such as $FeCO_3$ or $CaCO_3$. Swarf addition in precipitation is highly recommended to allow cementation of Ni and Co.

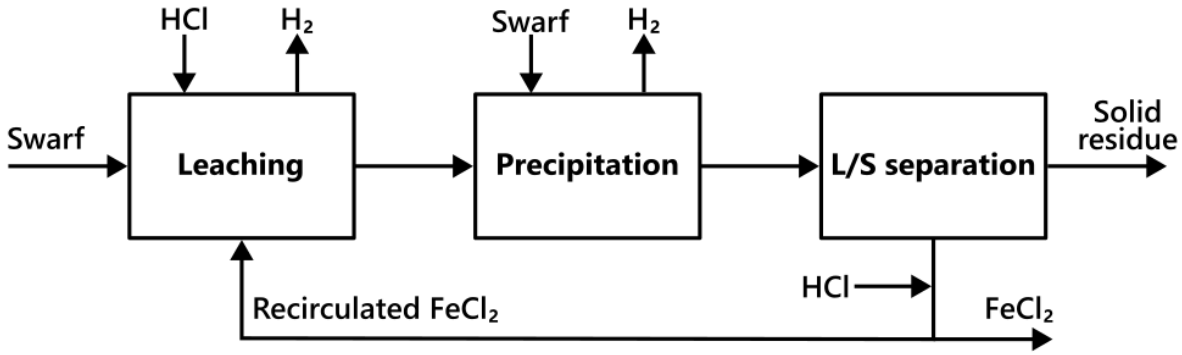

Figure 22: Flowsheet of the recycling process for producing $FeCl_2$ and hydrogen gas from steel swarf.

Concentrated hydrochloric acid (≥30%) and low L/S ratios are preferable in leaching to produce a more concentrated $FeCl_2$ solutions and ensure good contact areas for cementation. Thus far, an initial L/S=3 mL/g has been tested and proven to be acceptable in terms of mixing and foam formation. Initial liquid should be provided by recirculating $FeCl_2$ filtrate as this provides a leaching environment where cementation of impurities and lubricant coagulation and flocculation is optimal. Filtrate should be stabilized immediately by hydrochloric acid after L/S separation to avoid precipitation of iron oxides if the solution is contacted with air. With these operating conditions, it should be possible to obtain around 4 m^3, 40 wt-%, high purity $FeCl_2$ solution and 30 kg of H_2 per ton of swarf recycled.

Finally, the process is most easily operated in batch where the leaching and precipitation can be performed in a single reactor vessel. The tank should be closed for capturing a pure H_2 stream without air contamination. Likewise, filtration is also best done in an air free environment to avoid oxidation and precipitation of $FeCl_2$ in the filter cake. Glass, rubber or similar corrosion resistant equipment is required due to the extremely corrosive nature of hydrochloric acid and iron chloride solutions.

6 Summary and conclusions

The aim of this work was to investigate recycling of steel grinding swarf by producing a water treatment coagulant solution. Swarf was found to be highly heterogeneous, both in its day-to-day composition but especially between manufacturers, which called for a flexible, yet simple scheme to make recycling economical. Two swarf samples from different manufacturers were investigated for this purpose, each from grinding of low alloy bearing or chainsaw blade steels, using alumina grinding wheels and semi-synthetic cutting fluids.

A leaching process with hydrochloric acid was first optimized for grinding swarf from bearing manufacturing to study metal leaching at different temperatures, pH and L/S ratios. It was found that selective extraction of Fe and separation from Cr was possible at 60°C and pH 4 and that a relatively pure $FeCl_2$ solution could be obtained in a single leaching step. While L/S had a limited effect on Fe, leaching of Ni was inhibited at the lowest tested ratio of 20 mL/g. Regardless, Fe extraction was relatively inefficient at pH 4 and higher acidities were required to completely leach Fe. An alternative two-step process was therefore developed by splitting the dissolution process into a leaching and impurity precipitation step. By leaching at pH 2 for 3 h and consecutively raising pH to 4, ≥95 % extraction of Fe was possible with complete separation of Cr, Al and Mo via hydrolysis precipitation.

At this point, swarf from chainsaw blades manufacturing was subjected to the same leaching and precipitation and found to be more difficult to dissolve with only 50% Fe extraction. As this swarf was merely filtered beforehand and contained more cutting fluids than briquetted swarf from bearings, this behaviour was attributed to passivation of the steel surface by organic corrosion inhibitors. Emulsified oils and additives in the lubricants were found to be flocculated by solids during leaching and could thereby form a protective layer on the metal surface. It was concluded that further pretreatment of swarf by e.g. briquetting or centrifugation, after filtration of grinding sludges was necessary to facilitate leaching.

Further concentration of the leachate was required to match commercial 3.5 M $FeCl_3$. To do this, L/S ratios were minimized, and leachate was recirculated to stepwise increase $FeCl_2$ concentrations from 2.0 to 3.3 and finally 4.5 M. The leaching and precipitation performed relatively well with increasing concentrations apart from slightly slower leaching and difficulties with pH adjustment. When concentrating the solution, it was found that removal of Ni and Co by cementation was possible and was facilitated by high Cl^- concentrations.

Results from this work were put together in a flowsheet, designed for optimal separation of Fe from nonferrous metals and oils. The working principles should result in good separation of Cr, Ni, Cu, Co, Mo and Al from $FeCl_2$ and can potentially also remove other impurities, irrespective of the swarf composition. Besides high purity $FeCl_2$, the process also generated hydrogen gas and solid leaching residues with potential applications in the steel industry. Due to the high content of C and alloying elements such as Cr and Mo in residues, it was proposed as starting material for stainless steel production via recycling with other oxidized Fe wastes.

7 Future work

A primary goal in future work will be to present a complete recycling process for producing marketable $FeCl_3$ solutions from grinding swarf. So far, high purity $FeCl_2$ solutions have been produced and what remains is oxidation of Fe(II) and removal of any organic contaminants originating from cutting fluids. Industrially, Fe oxidation is achieved with oxygen, chlorate, etc. but this may not provide sufficiently oxidizing conditions for converting organic carbon to CO_2. As such, developing a flexible advanced oxidation process will be a main focus.

As discussed previously, hydrogen peroxide represents a possible candidate for oxidizing organic carbon via the Fenton process. Chemical oxidants however often have a poor sustainability profile and since the chemical oxygen demand is large as practically all Fe is unoxidized, this would likely result in a noncompetitive process in terms of sustainability. Electrochemical oxidation might present a more sustainable option as no additional chemicals would be needed. There may even be an opportunity to generate additional H_2 and scavenging metal impurities by electrowinning at the anode while oxidizing Fe(II) at the cathode.

This work has also shown that grinding swarf containing more cutting fluids are difficult to recycle using hydrometallurgy. Leaching of swarf containing straight or soluble oils would therefore also be of interest. Moreover, the influence of pretreatment methods like briquetting and centrifugation should be investigated further to evaluate the full potential of the proposed recycling process.

With a complete process in mind, techno economic analysis and life cycle assessment are key in determining the commercial potential and sustainability profile of the recycling process, including oxidation, compared with current $FeCl_3$ production routes. Techno economic aspects are currently explored via a startup company in collaboration with Chalmers School of Entrepreneurship. Environmental impact assessment will on the other hand be done as part of this research project.

Acknowledgements

I would first and foremost like to thank my supervisor Martina Petranikova for giving me so much freedom in my research and always leaving your door open whenever I needed counseling and guidance. This has been an ideal learning experience for me and I'm looking forward to another two years of working together. Thanks also to Christian Ekberg for introducing me to the wonderful world of solution chemistry and providing feedback in the writing process.

Special acknowledgement goes to Linda Widbro at SKF and Anders Krantz at Husqvarna for generously providing all the swarf I needed to continue my work. Our discussions and visits to the manufacturing sites have also been invaluable in giving a real-life perspective on manufacturing and waste management problems that the industry is facing. Peter Krajnik from Chalmers Industrial and Materials Science should also be recognized for kindly giving me insight into technical aspects of grinding processes.

I also want to thank the staff at Chalmers Innovations Office and Chalmers Ventures for daring me to take a step towards commercializing this research project. You have taken me out of my comfort zone and given me tons of new learning experiences. I'm also very grateful to get to work together with Ebba Adolfsson, Ta Huong Thao and Albin Frick from Chalmers School of Entrepreneurship. Your business development work has been amazing and even helped direct my research towards creating more realistic and sustainable solutions.

Finally, I could not have done this work without support from my wonderful partner Hanna. It is always comforting to know you are by my side and know that we have many great years ahead of us. Thanks also to all my lovely friends, family and colleagues at NC/IMR who I can always turn to in need and are there to provide the necessary fun activities outside of work.

This work was supported by the Swedish governmental research council for sustainable development Formas (Project number: 2021–00449).

Bibliography

[1] International Energy Agency. *Emissions Measurement and Data Collection for a Net Zero Steel Industry*. 2023.

[2] Conejo AN, Birat JP, Dutta A. A review of the current environmental challenges of the steel industry and its value chain. *J Environ Manage* 2020; 259: 109782.

[3] World Steel Association. *World Steel in Figures*. 2022.

[4] Lopez G, Farfan J, Breyer C. Trends in the global steel industry: Evolutionary projections and defossilisation pathways through power-to-steel. *J Clean Prod* 2022; 375: 134182.

[5] Pauliuk S, Milford RL, Müller DB, et al. The steel scrap age. *Environ Sci Technol* 2013; 47: 3448–3454.

[6] Liu W, Zuo H, Wang J, et al. The production and application of hydrogen in steel industry. *Int J Hydrogen Energy* 2021; 46: 10548–10569.

[7] Jernkontoret. Historia, Grundläggande metallurgi. In: *Järn- och stålframställning, utbildningspaket del 1*. 2016.

[8] World Steel Association. *Steel industry by-products project group report 2007 - 2009*. World Steel Ass, 2010.

[9] Alonso-Santurde R, Coz A, Viguri JR, et al. Recycling of foundry by-products in the ceramic industry: Green and core sand in clay bricks. *Constr Build Mater* 2012; 27: 97–106.

[10] Lee CM, Choi YH, Ha JH, et al. Eco-friendly technology for recycling of cutting fluids and metal chips: A review. *International Journal of Precision Engineering and Manufacturing - Green Technology* 2017; 4: 457–468.

[11] Fosnacht D. *Characterization and utilization of iron-bearing steel plant waste materials*.

[12] Wu X, Li C, Zhou Z, et al. Circulating purification of cutting fluid: an overview. *International Journal of Advanced Manufacturing Technology* 2021; 117: 2565–2600.

[13] European Commision.
Commission notice on technical guidance on the classification of waste. (2018/C 124/01), 2018.

[14] Hess MJ, Kawatra SK. Environmental Beneficiation of Machining Wastes-Part I: Material Characterization of Machining Swarf. *J Air Waste Manage Assoc* 1999; 49: 207–212.

[15] Großwendt F, Bürk V, Kopanka B, et al. A novel powder-metallurgical eco-friendly recycling process for tool steel grinding sludge. *J Clean Prod* 2023; 392: 136329.

[16] Chang JI, Lin JJ, Huang JS, et al. Recycling oil and steel from grinding swarf. *Resour Conserv Recycl* 2006; 49: 191–201.

[17] Brinksmeier E, Eckebrecht J, Buhr H. Improving ecological aspects of the grinding process by effective waste management. *Journal of Materials Processing Technology* 1994; 44: 171–178.

[18] Irani RA, Bauer RJ, Warkentin A. A review of cutting fluid application in the grinding process. *Int J Mach Tools Manuf* 2005; 45: 1696–1705.

[19] Hankel J, Jäger S, Weber S. Development of a recycling strategy for grinding sludge using supersolidus liquid phase sintering. *J Clean Prod* 2020; 263: 121501.

[20] Adler A, Yaniv I, Solter E, et al. Examining the role of cutting fluids in machining and efforts to adress associated environmental/health concerns. *Machining Science and Technology* 2006; 28: 23–28.

[21] Azarhoushang B. Abrasive tools. *Tribology and Fundamentals of Abrasive Machining Processes: Third Edition* 2022; 31–73.

[22] Azarhoushang B. Abrasives. *Tribology and Fundamentals of Abrasive Machining Processes: Third Edition* 2022; 3–30.

[23] Nakamura K, Hayashi S. Grinding Sludge Recycling to Reduce Environmental Load Analysis of Disturbing Factor for Briquetting of Grinding Sludge. *Tetsu-to-Hagane* 2006; 92: 535–538.

[24] Ottink T, Vieceli N, Foreman MRSJ, et al. Novel approach to recycling of steel swarf using hydrometallurgy. *Resour Conserv Recycl* 2022; 185: 106450.

[25] Nayström P. *Brikettering av stål-och gjutjärnspån samt slipmull*. 1998.

[26] Punmatharith T, Rachakornkij M, Imyim A, et al. Co-processing of grinding sludge as alternative raw material in portland cement clinker production. *Journal of Applied Sciences* 2010; 10: 1525–1535.

[27] Lee H, Jung M, Bae M, et al. Removal of oil from ferrous grinding swarf of automobile industry by aqueous washing process. *Waste Management* 2020; 111: 51–57.

[28] Fu H, Matthews MA, S. Warner L. Recycling steel from grinding swarf. *Waste Management* 1998; 18: 321–329.

[29] Ruffino B, Zanetti MC. Recycling of steel from grinding scraps: Reclamation plant design and cost analysis. *Resour Conserv Recycl* 2008; 52: 1315–1321.

[30] El Baradie MA. Cutting fluids: Part II. Recycling and clean machining. *J Mater Process Technol* 1996; 56: 798–806.

[31] El Samrani AG, Lartiges BS, Villiéras F. Chemical coagulation of combined sewer overflow: Heavy metal removal and treatment optimization. *Water Res* 2008; 42: 951–960.

[32] Amuda OS, Amoo IA. Coagulation/flocculation process and sludge conditioning in beverage industrial wastewater treatment. *J Hazard Mater* 2007; 141: 778–783.

[33] Jiang JQ. The role of coagulation in water treatment. *Curr Opin Chem Eng* 2015; 8: 36–44.

[34] Bratby J. *Coagulation and Flocculation in Water and Wastewater Treatment*. Third Edition. London: IWA publishing, 2016.

[35] Yin CY. Emerging usage of plant-based coagulants for water and wastewater treatment. *Process Biochemistry* 2010; 45: 1437–1444.

[36] Incopa. Iron-based coagulant: A good example of the circular economy. *2020*.

[37] Wildermuth E, Stark H, Friedrich G, et al. Iron Compounds. *Ullmann's Encyclopedia of Industrial Chemistry*. Epub ahead of print 15 June 2000. DOI: 10.1002/14356007.A14_591.

[38] Free ML. *Hydrometallurgy: Fundamentals and Applications*. Second Edition. Salt Lake City: Springer, 2021.

[39] Havlík T. *Hydrometallurgy Principles and Applications*. Woodhead Publishing, 2008. Epub ahead of print 2008. DOI: 10.1533/9781845694616.242.

[40] Baláž P. Mechanical activation in hydrometallurgy. *Int J Miner Process* 2003; 72: 341–354.

[41] Sipos P. Application of the Specific Ion Interaction Theory (SIT) for the ionic products of aqueous electrolyte solutions of very high concentrations. *J Mol Liq* 2008; 143: 13–16.

[42] Anderko A, Wang P, Rafal M. Electrolyte solutions: from thermodynamic and transport property models to the simulation of industrial processes. *Fluid Phase Equilib* 2002; 194–197: 123–142.

[43] Rowland D, Königsberger E, Hefter G, et al. Aqueous electrolyte solution modelling: Some limitations of the Pitzer equations. *Applied Geochemistry* 2015; 55: 170–183.

[44] Smith WR. COMPUTER SOFTWARE REVIEWS HSC Chemistry for Windows, 2.0, https://pubs.acs.org/sharingguidelines (1995, accessed 19 January 2024).

[45] Einar Mattsson. *Basic Corrosion Technology for Scientists and Engineers*. Second Edition. London: Maney Publishing for IOM3, the Institute of Materials, Minerals and Mining, 1996, 1996.

[46] Cappuyns V, Swennen R. The application of pHstat leaching tests to assess the pH-dependent release of trace metals from soils, sediments and waste materials. *J Hazard Mater* 2008; 158: 185–195.

[47] Larsson K, Ekberg C, Ødegaard-Jensen A. Dissolution and characterization of HEV NiMH batteries. *Waste Management* 2013; 33: 689–698.

[48] Montgomery DC. *Design and analysis of experiments*. 10th ed. John Wiley & Sons, 2020.

[49] Westcott C. *Ph Measurements*. Academic Press Inc, 1978.

[50] Morgan B, Lahav O. The effect of pH on the kinetics of spontaneous Fe(II) oxidation by O2 in aqueous solution – basic principles and a simple heuristic description. *Chemosphere* 2007; 68: 2080–2084.

[51] BASF SE Fuel and Lubricant Solutions. Amines for Metalworking Fluids.

[52] Niu Z, Li G, He D, et al. Resource-recycling and energy-saving innovation for iron removal in hydrometallurgy: Crystal transformation of ferric hydroxide precipitates by hydrothermal treatment. *J Hazard Mater* 2021; 416: 125972.

[53] Cannon P. The solubility of molybdenum trioxide in various mineral acids. *Journal of Inorganic and Nuclear Chemistry* 1959; 11: 124–127.

[54] XIAO F, ZHANG B, LEE C. Effects of low temperature on aluminum(III) hydrolysis: Theoretical and experimental studies. *Journal of Environmental Sciences* 2008; 20: 907–914.

[55] Sareyed-Dim NA. *The cementation of nickel onto iron at elevated temperatures*. Monash University, 1974.

[56] Addy S, Fletcher AJ. The deposition of cobalt on iron powder by means of the cementation reaction. *Hydrometallurgy* 1987; 17: 269–280.

[57] Miller JD, Beckstead LW. Surface deposit effects in the kinetics of copper cementation by iron. *Metallurgical Transactions* 1973; 4: 1967–1973.

[58] Rihan R, Shawabkeh R, Al-Bakr N. The effect of two amine-based corrosion inhibitors in improving the corrosion resistance of carbon steel in sea water. *J Mater Eng Perform* 2014; 23: 693–699.

[59] Ríos G, Pazos C, Coca J. Destabilization of cutting oil emulsions using inorganic salts as coagulants. *Colloids Surf A Physicochem Eng Asp* 1998; 138: 383–389.

[60] Guimarães AP, Maia DAS, Araújo RS, et al. Destabilization and Recuperability of Oil Used in the Formulation of Concentrated Emulsions and Cutting Fluids. *Chem Biochem Eng Q* 2010; 24: 43–49.

[61] Atkins P, de Paula J. *Atkins' Physical Chemistry*. Seventh Edition. Oxford University Press, 2002.

[62] Duan J, Gregory J. Coagulation by hydrolysing metal salts. *Adv Colloid Interface Sci* 2003; 100–102: 475–502.

[63] Fred Schimmel RA. The Ferrous Chloride-Water-Hydrogen Chloride System The Ternary Systems Ferrous Chloride-Hydrogen Chloride-Water, Ferric Chloride-Ferrous Chloride-Water. *J Am Chem Soc*; 74.

[64] Lienhardt WS. *Process of recovering nickel*. 1925.

[65] Saylam H. *Deposition of cobalt on iron powder*. Sheffield City Polytechnic, 1982.

[66] Winand R. Chloride hydrometallurgy. *Hydrometallurgy* 1991; 27: 285–316.

[67] Jinxing J. *Fundamental aspects of nickel electrowinning from chloride electrolytes*. The University of British Columbia, 1982.

[68] Hurlen T. Kinetics and thermodynamics of Ni/Ni(II) reactions in concentrated solutions of nickel and calcium chlorides. *Electrochim Acta* 1975; 20: 499–505.

[69] Johnsson J. *LLNL thermo database*. The Geochemists Workbench, 2000.

[70] Anacleto AL, Carvalho JR. Mercury cementation from chloride solutions using iron, zinc and aluminium. *Miner Eng* 1996; 9: 385–397.

[71] Makhloufi L, Saidani B, Hammache H. Removal of lead ions from acidic aqueous solutions by cementation on iron. *Water Res* 2000; 34: 2517–2524.

[72] Johansson K, Liljenroth A. *Carbon footprints of inorganic coagulants*. October 2023.

[73] Abdel-Fatah MA, Hawash SI, Shaarawy HH. Cost-effective Clean Electrochemical Preparation of Ferric Chloride and its Applications. *Egypt J Chem* 2021; 64: 3841–3851.

[74] Stucki S, Kötz R, Carcer B, et al. Electrochemical waste water treatment using high overvoltage anodes Part II: Anode performance and applications. *J Appl Electrochem* 1991; 21: 99–104.

[75] Silver J. *Chemistry of Iron*. Springer Netherlands, 1993. Epub ahead of print 1993. DOI: 10.1007/978-94-011-2140-8.

Supporting materials

Figures S1-S6 show Eh-pH diagrams for different metals found in grinding swarf, in aqueous chloride systems including only condensed and aqueous phases. The diagrams were created in HSC Chemistry 10 using the standard thermodynamic database and concentrations of 0.001 mol/kg water metal ion and chloride. Due to these low concentrations, the diagrams should only be used as a guideline for metal stability in the leaching process.

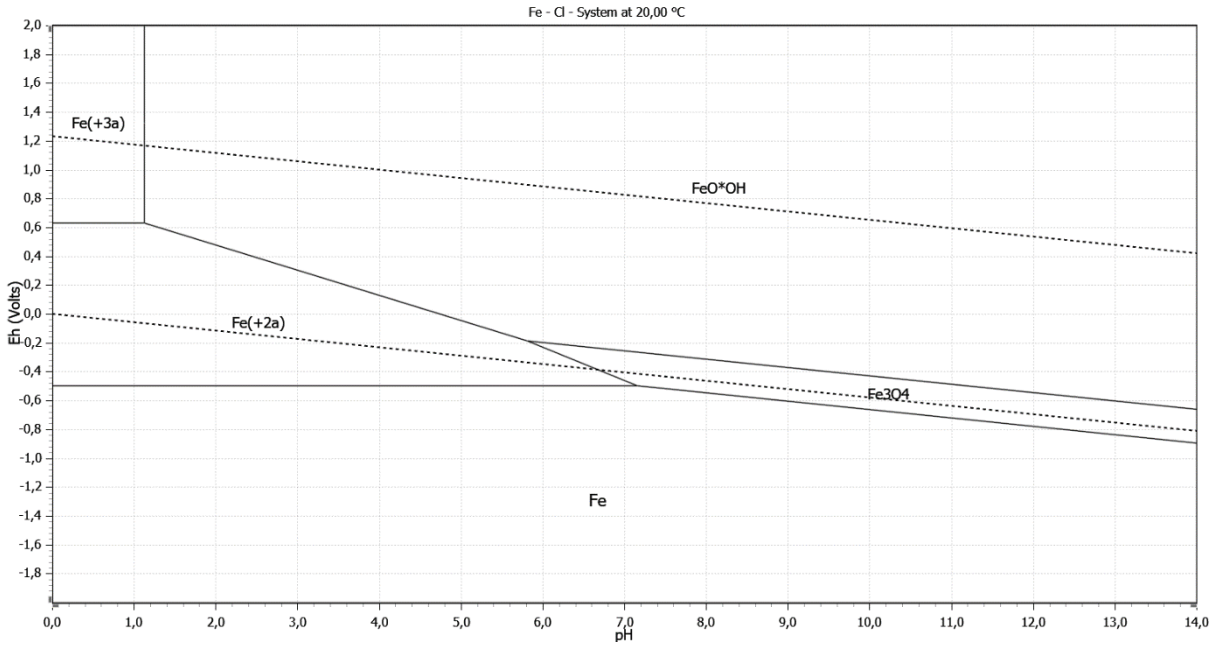

S1: Eh-pH diagram of Fe-Cl-H_2O with oxygen at low ionic strength (I < 0.01 M).

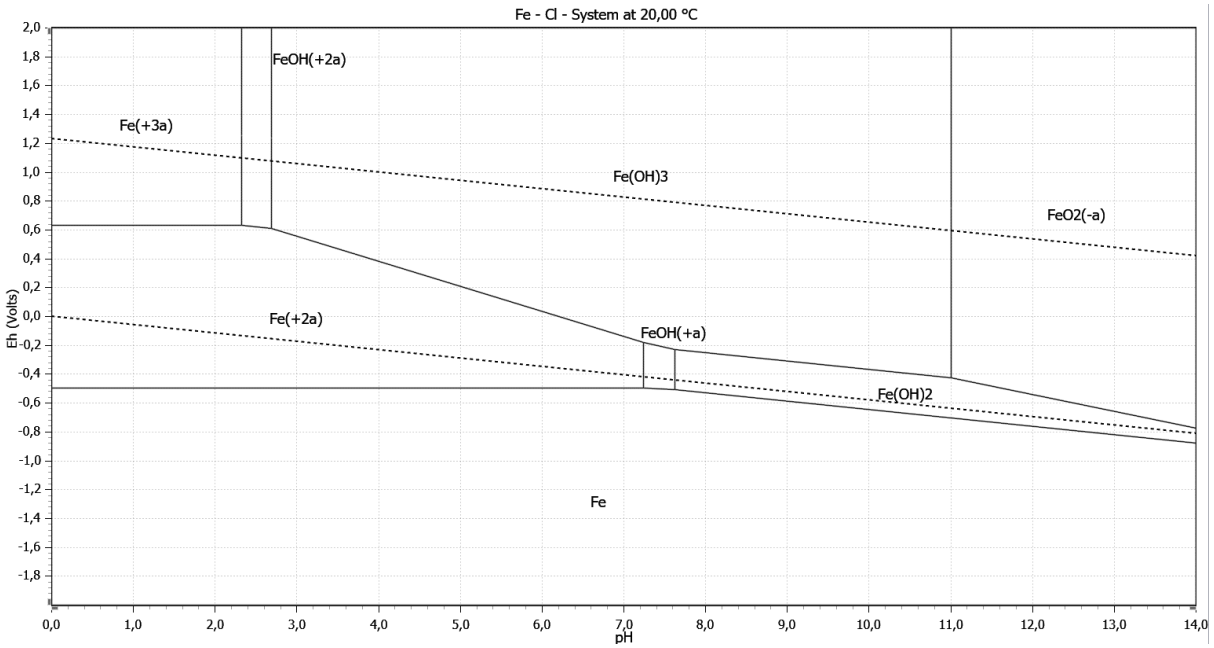

S2: Eh-pH diagram of Fe-Cl-H_2O under anoxic conditions at low ionic strength (I < 0.01 M).

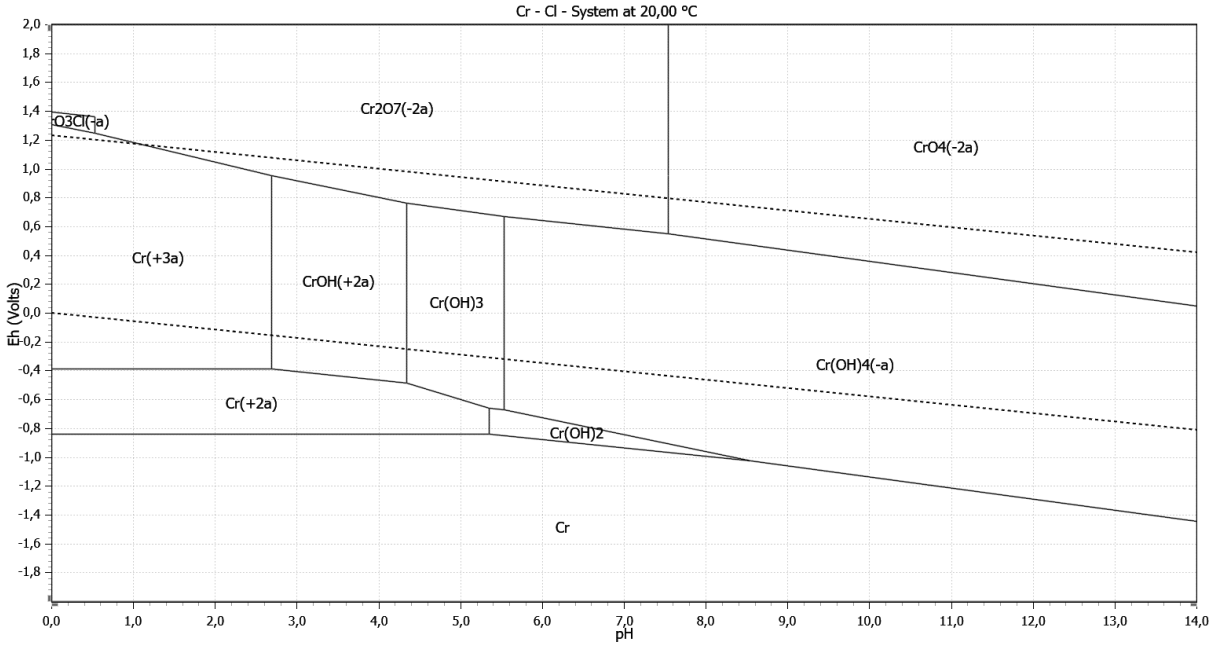

S3: Eh-pH diagram of Cr-Cl-H_2O at low ionic strength (I < 0.01 M).

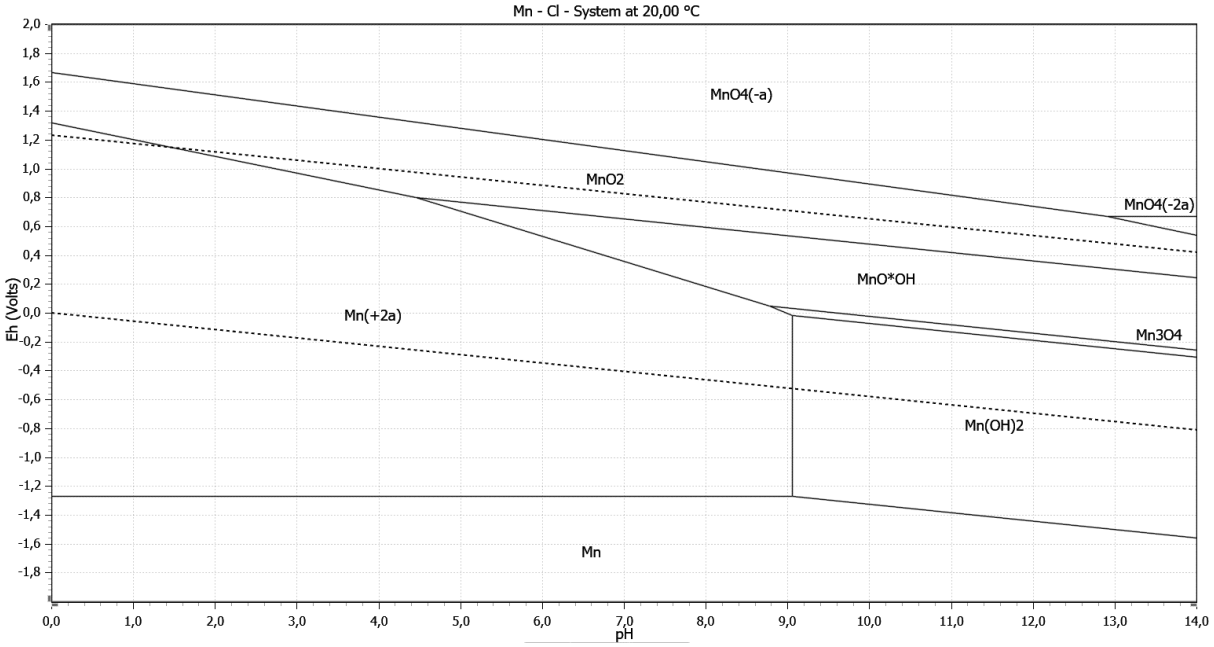

S4: Eh-pH diagram of Mn-Cl-H_2O at low ionic strength (I < 0.01 M).

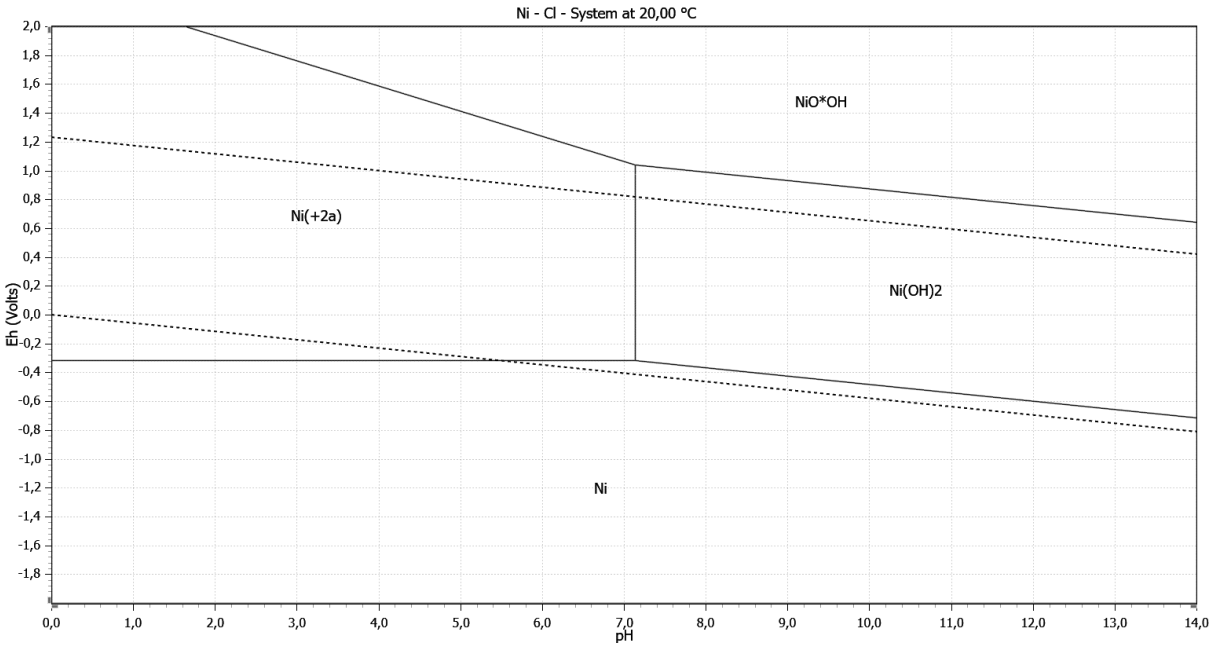

S5: Eh-pH diagram of Ni-Cl-H_2O at low ionic strength (I < 0.01 M).

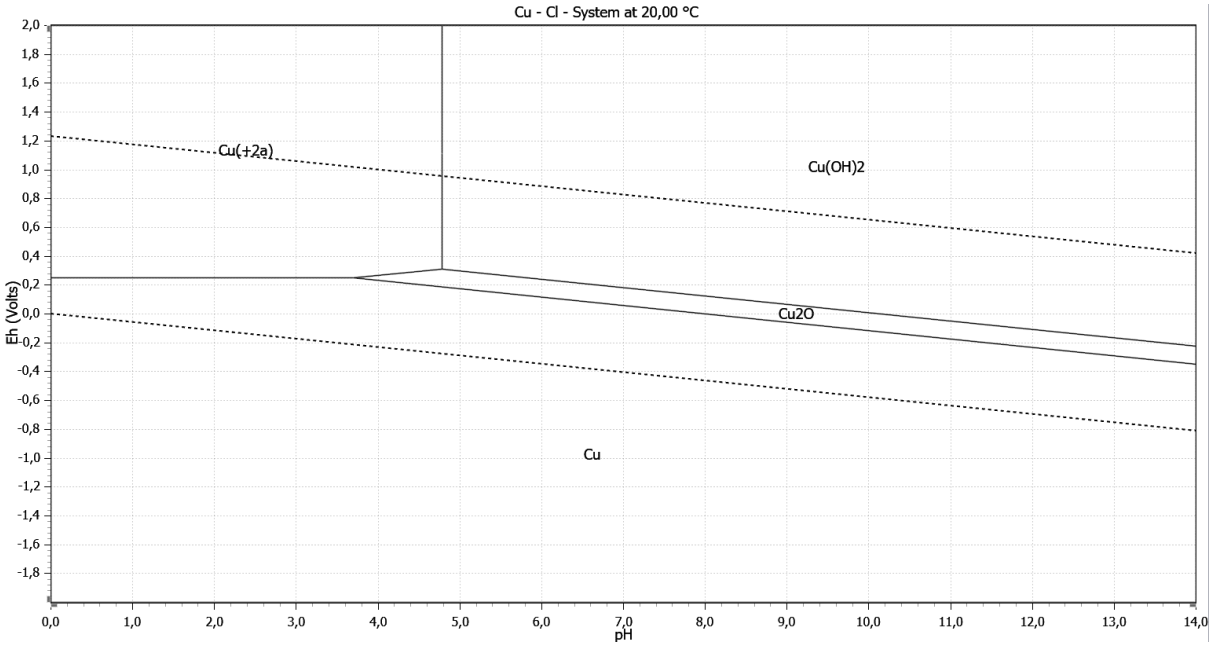

S6: Eh-pH diagram of Cu-Cl-H_2O at low ionic strength (I < 0.01 M).